Toxicology and Applied Pharmacology **183,** 23–40 (2002)
doi:10.1006/taap.2002.9451

Use of a Hybrid Computational Fluid Dynamics and Physiologically Based Inhalation Model for Interspecies Dosimetry Comparisons of Ester Vapors

Clay B. Frederick,*[,1] Larry G. Lomax,*[,2] Kurt A. Black,*[,3] Lavorgie Finch,* Harvey E. Scribner,* Julia S. Kimbell,† Kevin T. Morgan,†[,4] Ravi P. Subramaniam,†[,5] and John B. Morris‡

*Toxicology Department, Rohm and Haas Company, 727 Norristown Road, Spring House, Pennsylvania 19477; †CIIT Centers for Health Research, P.O. Box 12137, Research Triangle Park, North Carolina 27709; and ‡Toxicology Program, School of Pharmacy, University of Connecticut, Storrs, Connecticut 06269-2092

Received December 25, 2001; accepted April 20, 2002

Use of a Hybrid Computational Fluid Dynamics and Physiologically Based Inhalation Model for Interspecies Dosimetry Comparisons of Ester Vapors. Frederick, C. B., Lomax, L. G., Black, K. A., Finch, L., Scribner, H. E., Kimbell, J. S., Morgan, K.T., Subramaniam, R. P., and Morris, J. B. (2002). *Toxicol. Appl. Pharmacol.* **183, 23–40.**

Numerous inhalation studies have demonstrated that exposure to high concentrations of a wide range of volatile acids and esters results in cytotoxicity to the nasal olfactory epithelium. Previously, a hybrid computational fluid dynamics (CFD) and physiologically based pharmacokinetic (PBPK) dosimetry model was constructed to estimate the regional tissue dose of organic acids in the rodent and human nasal cavity. This study extends this methodology to a representative volatile organic ester, ethyl acrylate (EA). An *in vitro* **exposure of explants of rat olfactory epithelium to EA with and without an esterase inhibitor demonstrated that the organic acid, acrylic acid, released by nasal esterases is primarily responsible for the olfactory cytotoxicity. Estimates of the steady-state concentration of acrylic acid in olfactory tissue were made for the rat nasal cavity by using data from a series of short-term** *in vivo* **studies and from the results of CFD–PBPK computer modeling. Appropriate parameterization of the CFD–PBPK model for the human nasal cavity and to accommodate human systemic anatomy, metabolism, and physiology allowed interspecies dose comparisons. The CFD–PBPK model simulations indicate that the olfactory epithelium of the human nasal cavity is exposed to at least 18-fold lower tissue concentrations of acid released from EA than the olfactory epithelium of the rat nasal cavity under the same exposure conditions. The magnitude of this difference varies with the specific exposure scenario that is simulated and with the specific dataset of human esterase activity used for the simulations. The increased olfactory tissue dose in rats relative to humans may be attributed to both the vulnerable location of the rodent olfactory tissue (comprising greater than 50% of the nasal cavity) and the high concentration of rat olfactory esterase activity (comparable to liver esterase activity) relative to human olfactory tissue. These studies suggest that the human olfactory epithelium is protected from vapors of organic esters significantly better than rat olfactory epithelium due to substantive differences in nasal anatomy, nasal and systemic metabolism, systemic physiology, and air flow. Although the accumulation of acrylic acid in the nasal tissues may be a primary concern for nasal irritation and human risk assessment, acute animal inhalation studies to evaluate lethality (LD50-type studies) conducted at very high vapor concentrations of ethyl acrylate indicated that a different mechanism is primarily responsible for mortality. The rodent studies demonstrated that systemic tissue nonprotein sulfhydryl depletion is a primary cause of death at exposure concentrations more than two orders of magnitude above the concentrations that induce nasal irritation. The CFD–PBPK model adequately simulated the severe depletion of glutathione in systemic tissues (e.g., liver and lung) associated with acute inhalation exposures in the 500-1000 ppm range. These results indicate that the CFD–PBPK model can simulate both the low-dose nasal tissue dosimetry associated with irritation and the high-dose systemic tissue dosimetry associated with mortality. In addition, the comparison of simulation results for ethyl acetate and acetone to nasal deposition data suggests that the CFD–PBPK model has general utility as a tool for dosimetry estimates for a wide range of other esters and slowly metabolized vapors.**

Key Words: **physiologically based pharmacokinetic (PBPK); computational fluid dynamics (CFD); ethyl acrylate; acrylic acid; nasal cavity; olfactory; esterase; interspecies extrapolation; risk assessment.**

Many volatile organic acids and esters have been demonstrated to induce histopathological damage in the olfactory

[1] To whom correspondence should be addressed at Merck & Co., Inc., Department of Safety Assessment, WP45A-201, 770 Sumneytown Pike, P.O. Box 4, West Point, PA 19486. Fax: (215) 993-2190. E-mail: clay_frederick@merck.com.

[2] Current address: State of Arkansas Diagnostic Laboratory, 1 Natural Resources Drive, Little Rock, AR 72205.

[3] Current address: Merck & Co., Inc., Dept. of Safety Assessment, WP45–220, Sumneytown Pike, P.O. Box 4, West Point, PA 19486.

[4] Current address: Aventis Pharmaceuticals, 5016 Royal Dornoch Drive, Raleigh, NC 27604.

[5] Current address: U.S. EPA, NCEA, MD-8623D, 1200 Pennsylvania Ave., NW, Washington, DC 20460.

0041-008X/02 $35.00

epithelium in the nasal cavity of rodents in acute, subchronic, and chronic inhalation studies (e.g., Miller *et al.*, 1981, 1985; Keenan *et al.*, 1990; Trela and Bogdanffy, 1991; Hext *et al.*, 2001). Rarely does this olfactory damage extend to the adjacent respiratory epithelium (only with very strong acids such as formic acid; National Toxicology Program, 1992), even though the respiratory tissue lies closer to the nares and would be expected to receive a higher concentration of an inhaled vapor. Although this difference in tissue susceptibility is important for organic acids and esters, for inhaled vapors, the regional distribution of toxic effects generally has been correlated with the nasal air flow patterns. Typically, regions of high air flow exhibit a higher incidence and greater severity of toxic effects than regions of low air flow (Morgan and Monticello, 1990; Kimbell *et al.*, 1993, 1997; Mery *et al.*, 1994). Consequently, to provide a scientific basis for interspecies extrapolation and risk assessment for nasal toxicants, it is necessary to integrate the relevant data on species-specific anatomy, metabolism, air-flow patterns, and tissue susceptibility.

A prior study investigated the interspecies dosimetry of an organic acid vapor in the olfactory epithelium (Frederick *et al.*, 1998) by incorporating the development and use of a hybrid computational fluid dynamics (CFD) and physiologically based pharmacokinetic (PBPK) dosimetry model to estimate the regional tissue dose of organic acids in the rodent and human nasal cavity. Volatile organic acids are generally very water soluble and are typically metabolized relatively slowly by tissues in the respiratory tract. In contrast, organic esters are generally relatively poorly water soluble and are rapidly metabolized by esterases in respiratory tissues to release acids and alcohols (e.g., Bogdanffy *et al.*, 1987; Dahl *et al.*, 1987; Frederick *et al.*, 1992, 1994b; Mainwaring *et al.*, 2001). This study includes modification of the previously developed CFD–PBPK model to incorporate the metabolism of a representative organic ester, ethyl acrylate (EA), by nasal and systemic esterases. In addition, an *in vitro* study was conducted with explants of nasal tissue to determine whether it was the ester or its acid metabolite, acrylic acid, that was responsible for inducing the cytotoxicity that was observed in the sustentacular cells of the olfactory tissue.

The design criteria for the CFD–PBPK model used in this study were based on the observations from numerous laboratories on the parameters that generally determine regional and whole-nose nasal tissue dose (summarized in Frederick *et al.*, 1994a). These criteria specify a model that will provide simulation results such as a decreased fractional deposition of a vapor in the overall nasal cavity with an increase in inhalation flow rate, a decrease in the fractional nasal deposition of a vapor when the rate of nasal metabolism of the vapor is inhibited, and a decrease in the rate of nasal uptake of a poorly metabolized inhaled vapor as a function of time in extended exposure scenarios as the arterial blood concentration increases due to systemic loading of the vapor. To meet these design criteria, the structure of the hybrid CFD–PBPK model links the data from CFD simulations of air flow in the upper respiratory tract with a compartmental PBPK model. The PBPK part of the model has the the capacity to describe systemic distribution, metabolism, and excretion as well as systemic target tissue dose. The PBPK simulation of systemic metabolism and blood concentration is an important feature that allows the simulation of "back pressure" of poorly metabolized vapors that accumulate in the blood and inhibit the flux into the nasal tissue. In addition, the modeling of the circulatory system allows estimation of the accumulation and recirculation of metabolites of toxicological interest in the blood. Notably, as described below, the incorporation of systemic metabolism and the description of the systemic blood concentration of both the inhaled vapor and its major metabolite are critical features of this hybrid CFD–PBPK model for interspecies dose comparisons in both nasal and systemic tissues. This general model structure appears to be useful for tissue dose estimates and interspecies extrapolation for a wide range of inhaled vapors and for multiple toxicological endpoints, and it provides a scientific basis for tissue dose comparisons, interspecies extrapolation, and risk assessment. In keeping with the design philosophy used for the prior acid vapor model, the ester CFD–PBPK model is constructed and used with direct input of experimental data for the model parameters and without "fitting" or optimization of the parameters.

MATERIALS AND METHODS

Chemicals. Ethyl acrylate (CAS 140−88-5; Rohm and Haas Co., Bristol, PA) with a purity of >99.9% with 15 ppm 4-methoxyphenol to prevent polymerization was used for the study.

Acute inhalation exposure of rats. Male F344/N rats (approximately 60 to 75 days old upon arrival; weight range of 160 to 175 g 1 day prior to exposure) were obtained from Charles River Laboratories (Wilmington, MA). Food and filtered tap water were supplied *ad libitum*, except during inhalation exposure, when food and water were withheld. The animals (five per group for immediate histopathological evaluation, five per group for histopathological evaluation after a 6-week recovery period, and five per group for immediate analysis of tissue nonprotein sulfhydryl concentration) were administered a single, nose-only inhalation exposure of 0, 5, 25, or 75 ppm EA vapor for 1, 3, or 6 h (exposure concentrations based on subchronic and chronic bioassay histopathology reported by Miller *et al.*, 1985). Immediately following exposure, the animals were removed from the inhalation apparatus, anesthetized with sodium pentobarbital, and then killed by exsanguination by cutting the abdominal aorta. The nasal cavity of each animal designated for histopathological evaluation was infused with 10% neutral-buffered formalin via the pharyngeal duct and the head was then immersed and fixed in formalin, decalcified, and sectioned transversely at Levels I through IV (Young, 1981). The tissue sections were processed, microtomed at 4 to 6 μm, stained with hematoxylin and eosin, and evaluated for histopathology. Lesions were characterized according to the scheme used previously (Lomax *et al.*, 1994), and their locations were mapped according to the scheme described by Mery *et al.* (1994). A composite regional map was also constructed for each group. The recording of lesions was designed to qualitatively assess the extent, nasal region affected, and type of histologic lesions within the nasal cavity. In addition to the animals evaluated for histopathology immediately following inhalation exposure, additional groups of rats (five per group) were allowed to recover for 6 weeks prior to histopathological evaluation as described above.

In addition to the animals evaluated for nasal histopathology, additional

animals were evaluated for regional nasal tissue nonprotein sulfhydryl (NPSH) concentration. Following scheduled euthanasia as described above, the rat skull was carefully opened along the midline and the following nasal cavity tissues were collected, weighed in tared containers, and immediately frozen with dry ice for subsequent NPSH analysis: respiratory epithelium of the septum, respiratory epithelium of the lateral walls, olfactory epithelium of the dorsal meatus region, olfactory epithelium of the septum, and olfactory epithelium of the ethmoid turbinates. The collected tissues were stored at less than −50°C until NPSH analysis with Ellman's reagent using a microplate reader as previously described (Potter *et al.*, 1995).

In vitro incubation of nasal explants with ethyl acrylate. Nasal septa were carefully collected from female F344/N rats (weight range of 150 to 225 g) and incubated for 2 h in DMEM/F12 media supplemented with antibiotics (penicillin, streptomycin, and nystatin), insulin, transferrin, selenium, hydrocortisone, and epidermal growth factor under an atmosphere of 95% O_2 and 5% CO_2 at 37°C. For treated tissues, 0.06–3.6 mM EA was added to the medium prior to the addition of the tissues, and the treated medium was adjusted to pH 7.3 with 1 N sodium hydroxide. After incubation, the tissues were fixed with formalin, decalcified, imbedded in glycol methacrylate, microtomed at 2 to 3 μm, stained with hematoxylin and eosin, and evaluated for histopathology. An experiment was also conducted with 25 μM paraoxon in the culture medium to investigate the effects of inhibiting tissue esterase activity on the histopathological effects.

Human and monkey esterase activity. Human tissues were obtained from the International Institute for the Advancement of Medicine (IIAM). The tissues were obtained from IIAM on the same day as tissue collection using a quick courier service for transport and delivery. The tissues obtained from IIAM were normal tissues (e.g., excess surgical tissues or brain dead cadaver tissues) that were snap frozen in liquid nitrogen as soon as possible after collection. The tissues were packed in dry ice prior to shipping. Upon receipt, the samples were inventoried, transferred, and stored in a freezer maintained at less than or equal to −70°C, and ultimately thawed, homogenized, dialyzed, and used for determination of esterase activity (method described by Frederick *et al.*, 1992) and analysis of tissue glutathione concentration (microtiter plate Ellman's assay described by Potter *et al.*, 1995). Age and personal information were not available for the tissue donors. Sufficient tissue for determination of Michaelis–Menten parameters varied for each tissue, with tissues and kinetic determinations given in parentheses: liver (n = 5), lung (n = 5), kidney (n = 2), nasal respiratory epithelium (n = 5), nasal olfactory epithelium (n = 4), esophagus (n = 3), stomach (n = 2), and blood (n = 3). In addition to the human tissue samples, tissues were collected immediately following euthanasiz (phenobarbital overdose followed by exsanguination) from three cynomolgus monkeys. All tissues were wrapped in aluminum foil and snap frozen in liquid nitrogen immediately after collection, shipped on dry ice, and stored at less than or equal to −70°C until esterase determination and glutathione analysis was conducted by the same methods used for the human tissues.

Evaluation of glutathione transferase activity in nasal tissues. The enzymatic augmentation of the rate of conjugation of ethyl acrylate with glutathione by glutathione transferases in olfactory and respiratory epithelium was evaluated based on the method of Aceto *et al.* (1993). The reactions were conducted in 1.5-ml septum-sealed HPLC autoinjector vials in a total volume of 1.0 ml. The incubation mixtures contained 0.1 M sodium phosphate buffer (pH 7.3), with or without 25 mg protein from male Fisher F344/N rat nasal mucosa tissue homogenate (either olfactory homogenate or respiratory homogenate), 10 mM glutathione, 9 mM paraoxon (to inhibit esterase activity), and either 0.5 or 5.0 mM [1-^{14}C] ethyl acrylate (specific activity = 41.5 dpm/nmol). Reactions were initiated by the addition of substrate, incubated at 37°C for either 2.5, 5.0, 7.5, or 10 min, and then terminated by the addition of 100 μl of 10% phosphoric acid. Following centrifugation, the amount of radiolabeled glutathione–ethyl acrylate conjugate was quantified by HPLC with a flow radiation monitor. The amount of conjugate formed in the presence of enzyme was compared to the amount formed in the absence of enzyme as a measure of the enzymatic augmentation of the reaction rate.

Structure of the CFD–PBPK inhalation model. The CFD–PBPK model used for this study was composed of a whole-body compartmental physiologically based inhalation model that was constructed with the simulation language ACSL (Aegis Technologies Group, Inc., Huntsville, AL), with a nasal cavity as a port of entry for inhaled vapors. The basic structure of the CFD–PBPK model has been described in detail (Bush *et al.*, 1998; Frederick *et al.*, 1998). As previously described, the model recreates the CFD simulations used to parameterize it for both the rat and human nasal cavity when used to simulate "concentration = 0" boundary conditions for the nasal mucosa. For the ester model, the ionization components of the acid model were deleted and the model was modified to include the chemical-specific parameters for EA, a Michaelis–Menten description of tissue esterase activity for both rat and human, a description of steady-state tissue glutathione concentration and the second-order conjugation of the unsaturated ester by glutathione, a kidney compartment to describe renal metabolism and urinary excretion of released acrylic acid, and a description of oral breathing that bypasses the nasal cavity to simulate the breathing pattern of high work loads. The ester model includes a "nested" PBPK description of the metabolic formation of the acid released by the esterase, diffusion and distribution of the acid, and metabolism of the acid (cf. the PBPK model described for acrylic acid by Frederick *et al.*, 1998, except that systemic acrylic acid exposure is described by metabolic release rather than inhalation exposure; similar nested acid metabolite models have been described by Gargas *et al.*, 2000a,b and Hays *et al.*, 2000). The CFD–PBPK ester model is described in more detail in the Appendix, with a listing of model parameters and their sources. Cyclic flow simulations of breathing were conducted by alternately reversing air flow to simulate inhaling and exhaling. The regional distribution of air flow on exhalation was modeled by reversing the air flow determined by the CFD simulations of unidirectional flow of inhaled air. Although this assumption may introduce an error into cyclic flow simulations, the magnitude of this error is unknown. When additional CFD data become available, the model is structured so that it may be easily modified to incorporate regional differences in air flow patterns and gas-phase mass transfer between inhalation and exhalation.

Conceptually, the model could be constructed with any number of luminal/regional compartments. For this study, the interspecies comparisons were conducted with a relatively simple anatomically based compartmental model defined primarily by the epithelial types lining various regions of the nasal cavity and by the air flow patterns in the nasal cavity defined by the results of CFD simulations (Figs. 1 and 2). The flow of inhaled air across these regions is described in detail by Kimbell *et al.* (1993, 1997) for the rat nasal cavity and by Keyhani *et al.* (1995) and Subramaniam *et al.* (1998) for the human nasal cavity. Deposition of an inhaled vapor was governed by inhaled air flowing across the nasal vestibule, a dorsal medial airstream flowing over respiratory epithelium and then olfactory epithelium, and a second composite ventral and lateral air stream flowing over the remaining respiratory epithelium in the nasal cavity (divided into anterior and posterior compartments). All air from the nasal cavity then passes over a pharynx compartment before entering a composite lower respiratory tract compartment (which could be further subdivided into additional compartments for regional dose estimates, if necessary). Oral breathing is described by deposition of the fraction of air entering the oral cavity (along with any inhaled vapor) into the air space of the pharynx and by mixing of the fractions of orally and nasally inspired air in this region. The model does not currently subdivide the pharynx into regions (e.g., nasopharynx, oropharynx, and laryngopharynx) or describe the conducting airways, although these regions could be added after suitable CFD modeling.

The large olfactory region of rodents was divided into two compartments (Figs. 1 and 2): a small dorsal anterior compartment (13% of the olfactory epithelium and 7% of the total nasal surface area) and a large compartment representing the remaining olfactory epithelium on the septum and ethmoid turbinates (data from nasal CFD mesh and Gross *et al.*, 1982). The human nasal cavity (Figs. 1 and 2) does not have an anatomical equivalent for the rat ethmoid turbinates that are covered primarily with olfactory epithelium; consequently, the small human olfactory epithelium was described by one compartment comprising approximately 4% of the total nasal surface area (Lang, 1989).

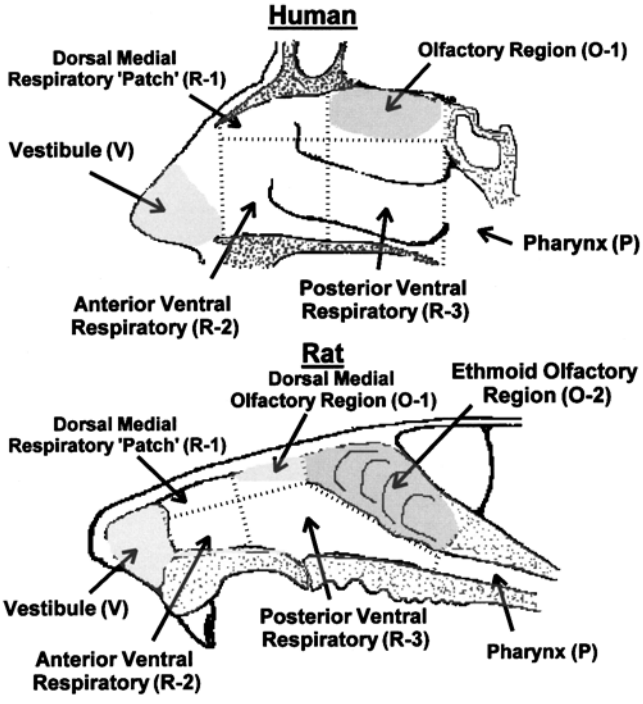

FIG. 1. Rat and human nasal anatomy divided into compartments corresponding to the epithelium lining the lumen. These compartments provide the basis for the CFD–PBPK model described in Fig. 2. The figure of the human nasal cavity was modified from Lang (1989) and the figure of the rat nasal cavity was modified from Miller *et al.* (1993).

The anatomical description of the epithelial tissue lining the nasal lumen in each region is the same as previously described (Frederick *et al.*, 1998; Fig. 3). Respiratory epithelium is described by two epithelial cell layers and the thicker olfactory epithelium is described by four cell layers. Nasal esterase activity (Frederick *et al.*, 1994b) was allocated to the appropriate cell layers according to the histochemistry and immunohistochemistry that has previously been reported (Bogdanffy *et al.*, 1987; Olson *et al.*, 1993; Lewis *et al.*, 1994; Mainwaring *et al.*, 2001). An adjustment in the V_{max} used in the Michaelis–Menten description of esterase activity used in the model was made to accommodate dilution of the enzymatically rich cell layers with cell layers deficient in esterase activity based on concerns raised by Bogdanffy *et al.* (1998). The dilution factors (four for respiratory epithelium and two for olfactory epithelium) were estimated based on microscopic evaluation of representative nasal epithelial tissue samples that had been collected as if they were to be homogenized and also by comparison with published photomicrographs (particularly, Olson *et al.*, 1993 and Mainwaring *et al.*, 2001). Esterase activity for the nasal cavity and systemic tissues was parameterized appropriately for each species based on previously published enzyme kinetic data (Frederick *et al.*, 1992, 1994b) and from kinetic data on tissues collected for this study. Systemic tissues were modeled as well-mixed compartments with uniform enzyme activity.

Second-order conjugation with glutathione was modeled in each nasal epithelial layer with steady-state glutathione synthesis based on previously published studies (Potter and Tran, 1993; Potter *et al.*, 1995). The rate of glutathione conjugation was increased 15-fold in the liver compartment to accommodate the augmentation of the reaction rate in this tissue by glutathione transferases (Potter and Tran, 1993). Otherwise, the available data indicate that glutathione transferases do not significantly enhance the rate of conjugation of ethyl acrylate with glutathione in most other tissues under physiological conditions (Potter and Tran, 1993). The data generated in this study (see below) indicated that nasal glutathione transferases do not contribute significantly to the ambient conjugation rate of ethyl acrylate with glutathione in nasal tissues. Initial tissue glutathione concentrations (which approximate tissue nonprotein sulfhydryl concentrations) were based on previously published data for rat tissues studies (Potter and Tran, 1993; Potter *et al.*, 1995). Additional data were collected on nonprotein sulfhydryl concentrations for selected human and monkey tissues.

Conduct of simulations with the CFD–PBPK inhalation model. The CFD–PBPK model simulates both unidirectional flow and cyclic breathing conditions. A prior study has evaluated the relationship between using the related acid CFD–PBPK model in unidirectional flow mode relative to cyclic flow mode (Andersen *et al.*, 2000). The problem with exercising the model in cyclic flow mode to simulate rat breathing is that it is very computationally intensive. For example, the average breathing time of a rat is approximately 0.4 s per breath, so a 4-h simulation of cyclic breathing involves modeling 36,000 inhalation and 36,000 exhalation events. Andersen *et al.* (2000) demonstrated that modeling extended exposures with unidirectional flow at a flow rate equal to the minute volume (effectively the time-weighted average inspiration flow rate) provided dosimetry estimates that were sufficiently accurate for interspecies dose comparisons. Based on these considerations, the long-term simulations of *in vivo* exposures to estimate systemic tissue concentrations were conducted under unidirectional flow conditions at an inspiration flow rate equal to the minute volume with the appropriate air flow distribution and mass transport coefficients for cyclic flow. However, estimates of nasal tissue concentrations were based on 1-h cyclic flow simulations since trial cyclic flow simulations up to 6 h indicated that steady-state conditions had been reached prior to 1 h.

To model human physiology in the workplace, CFD simulations were conducted as previously described (Frederick *et al.*, 1998; Subramaniam *et al.*, 1998) to derive the appropriate mass transport coefficients for the CFD–PBPK model. The CFD simulations were conducted at a flow rate of 35 L/min, which approximates the inspiratory flow rate associated with a work load of 50 W (Chadha *et al.*, 1987). The data for the compartmental air flow distribution and gas phase mass transport coefficients calculated from the 35 l/min CFD simulations are listed in the Appendix. In addition, the switch of humans from nasal breathing to oronasal breathing as a function of increasing work load has been evaluated in several laboratories (e.g., Niinimaa *et al.*, 1980, 1981; Chadha *et al.*, 1987; Wheatley *et al.*, 1991; Fregosi and Lansing, 1995; James *et al.*, 1997). To accommodate the results of these studies, an oral shunt of air flow into the pharynx was included in the model, assuming negligible absorption in the oral cavity. The parameters used for the switch from nasal to a combination of oral and nasal breathing were derived from Chadha *et al.* (1987), since this study reports the most detailed data on the relationship of workload to minute volume to the percentage of nasal breathing. Simulations of light working conditions were conducted both with and without an oral breathing component.

RESULTS

Nasal Histopathology Following Acute Inhalation Exposure of Rats to Ethyl Acrylate

An acute nose-only inhalation study (single exposure for 1, 3, or 6 h) was conducted at vapor concentrations with 0, 5, 25, and 75 ppm ethyl acrylate to evaluate the initial regional distribution of cytotoxic lesions induced in the rat nasal cavity. The olfactory epithelium was the only tissue in the nasal cavity that was affected by inhalation exposure to EA at 25 or 75 ppm for 3 or 6 h (Table 1). No effects were observed following 1 h of exposure at any of the tested exposure concentrations or at 0 or 5 ppm for any of the exposure periods. After 3 h of exposure to 25 ppm EA, two-fifth of rats had unilateral sustentacular cell necrosis and olfactory neuron degeneration and desquamation located on the lateral wall of the dorsal meatus

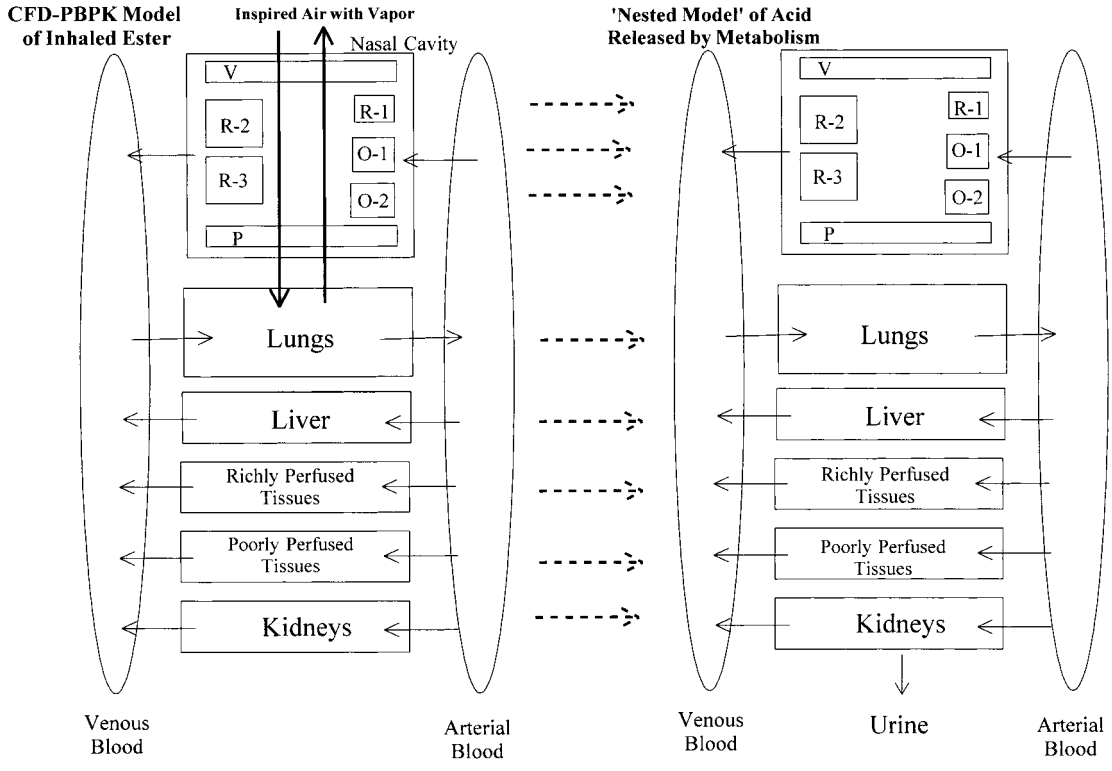

FIG. 2. Diagram of the CFD–PBPK model constructed to comprehensively describe the disposition of inhaled ethyl acrylate vapors. The rodent model divides the extensive olfactory region into two compartments. The anterior compartment describes the olfactory epithelium in the projection along the dorsal meatus. This is typically the initial target site for histopathological effects with increasing dose and/or exposure time of organic acids and esters. The human model uses one olfactory compartment since the human nasal cavity lacks a counterpart for the rodent ethmoid olfactory region.

in section III (Young, 1981). The histopathology of the lesions was essentially identical to that previously reported in a similar acute inhalation study with acrylic acid (Frederick *et al.*, 1998). No lesions were observed in sections IV and V. Exposure to 75 ppm EA for 3 h or to either 25 or 75 ppm for 6 h extended the distribution and severity of the olfactory lesions in the nasal cavity (Table 1). Bilateral sustentacular cell necrosis and olfactory neuron degeneration and desquamation extended into sections IV and V, and lesions were located across the majority of the dorsal meatus, in the dorsal regions of the septum, and on the lamellae of endoturbinate I. Affected animals in the 25-and 75-ppm exposure groups demonstrated almost complete recovery of normal olfactory tissue following a 6-week recovery period. Some animals exhibited occasional neuroepithelial rosette-like structures in areas that had previously been demonstrated to have histopathological damage. These structures were interpreted as evidence for ongoing regeneration of the olfactory neuroepithelium.

Regional Nonprotein Sulfhydryl Depletion in the Nasal Cavity Following Acute Inhalation Exposure of Rats to Ethyl Acrylate

Additional rats acutely exposed to ethyl acrylate vapor as described above were evaluated for the depletion of NPSH (primarily glutathione) in the nasal cavity. Epithelium was collected from the following regions of the nasal cavity (cf. Fig. 1): respiratory epithelium from the septum, respiratory epithelium from the lateral walls of the nasal lumen, olfactory epithelium lining the anterior dorsal meatus, olfactory epithelium from the septum, and olfactory epithelium from the ethmoid turbinates. The data (Table 2) indicate that inhalation exposure to ethyl acrylate can deplete NPSH content in both respiratory and olfactory epithelium. The magnitude of the response increased with exposure time and concentration. More extensive depletion was observed in the olfactory epithelium lining the dorsal meatus and the ethmoid turbinates than other regions of the nasal cavity, but the concurrent cytotoxicity observed in these regions may have been responsible for the loss of NPSH. Given extensive NPSH depletion in the respiratory epithelium in the absence of histopathological effects, it may be inferred that that NPSH depletion in the range observed is not sufficient to induce histopathological effects in this tissue.

In Vitro Incubation of Nasal Explants with Ethyl Acrylate

Short-term organ culture of nasal explants with media containing ethyl acrylate resulted in histopathological lesions very similar to those observed *in vivo* and to those previously

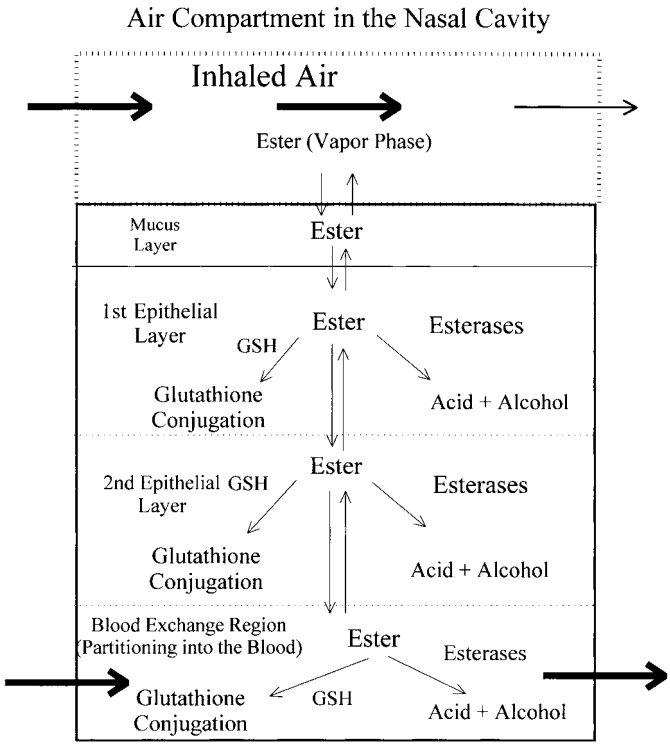

FIG. 3. Description of the way that the CFD–PBPK model represents the interaction of an unsaturated organic vapor with a region of epithelium lining the nasal cavity. The acid released by the esterases is also modeled as diffusing and being metabolized. The absorbed vapor that reaches the blood-exchange region underlying the nasal epithelial layers may be metabolized or it may partition into the venous blood and be transported systemically.

reported for a similar study with acrylic acid (Frederick *et al.*, 1998). The histopathological indications of cytotoxicity increased with increasing EA concentration (Table 3) and were first manifest as vacuolation and nuclear swelling of the sustentacular cells (Fig. 4) followed by sloughing of sustentacular and neuronal cells at higher concentrations. As a first-order approximation, the concentration of ethyl acrylate in the tissue explants may be estimated from the exposure concentration of ethyl acrylate in the medium (an upper bound estimate due to metabolism of the ester by the tissue). This would suggest that the steady-state tissue concentration of ethyl acrylate required to induce sustentacular cell cytotoxicity and subsequent loss of neuronal cells was $\leq$0.3 mM, with more severe toxicity characterized by the acute loss of sustentacular and neuronal cells observed at *in vitro* at tissue concentrations $\leq$3.6 mM. An ethyl acrylate concentration of 0.06 mM in the medium (and consequently an upper-bound concentration in the tissue) was a no-observed-adverse-effect level in this assay. No cytotoxicity was observed in the respiratory epithelium, suggesting that the ethyl acrylate tissue concentration required to induce cytotoxicity in respiratory epithelium in this assay was in excess of 3.6 mM.

A second experiment explored the effect of an esterase inhibitor (paraoxon) on the histopathological effects observed in the explants exposed to EA. These results (Table 4) indicate that paraoxon significantly inhibits the histopathological effects induced by EA in the olfactory sustentacular cells. No toxicity was seen in explants exposed to paraoxon alone. These data indicate that the acrylic acid that is released upon hydrolysis of EA in explants is the dominant factor that is causally related to the cytotoxic effects observed when olfactory tissue is exposed to relatively high concentrations of EA *in vitro*.

Human and Monkey Tissue Esterase Activity

The Michaelis–Menten rate constants for the hydrolysis of EA by homogenates of a range of human tissues were determined and compared to previously determined values for rat tissues (methodology and results described in Frederick *et al.*, 1992, 1994) (Table 5). The collection of human olfactory tissue is difficult due to its lack of availability and lack of accessibility. To gain additional data on the rates of esterase-catalyzed EA hydrolysis in primates, tissues were also collected from *Cynomolgous* monkeys immediately following euthanasia and evaluated for esterase activity. The monkey data were reasonably consistent with the limited human tissue data (Table 5).

Human and Monkey Nonprotein Sulfhydryl Concentration and the Evaluation of Glutathione Transferase Activity in Nasal Tissues

Data on the tissue concentrations of nonprotein sulfhydryl concentrations were collected for selected tissues from humans and monkeys (Table 6) and compared to previously collected data from rats (Potter and Tran, 1993; Potter *et al.*, 1995). The determination of the NPSH concentration includes all of the low-molecular-weight thiols in the tissue, but the major components are glutathione (the predominant constituent) and cysteine (Potter and Tran, 1993). Reasonable consistency in NPSH concentration was observed across species for the major organs. An exception was the human nasal tissues, which had relatively low concentrations of NPSH relative to rats. This was attributed to the long lag time between tissue collection and the conduct of the assay for the human tissues relative to the rat tissues.

The enzymatic augmentation of the rate of glutathione conjugation of ethyl acrylate by rat nasal tissue (either olfactory or respiratory) at pH 7.3 and 37°C was 10% or less. These results were consistent with the results previously reported by Potter and Tran (1993) for most epithelial tissues. Consequently, enzymatic augmentation of the nonenzymatic conjugation rate was not included in the model for the nasal tissues.

Comparison of the Output of the CFD–PBPK Rat Model to Rat Nasal Deposition Data

The CFD–PBPK was used to simulate the fractional deposition of ethyl acrylate in unidirectional flow experiments conducted with the surgically isolated rat nasal cavity (fractional

TABLE 1
Summary of Histopathology Findings by Nasal Cavity Region[a] with Exposure Time and Vapor Concentration Following a Single Nose-Only Inhalation Exposure to Ethyl Acrylate

	0 ppm EA hours			5 ppm EA hours			25 ppm EA hours			75 ppm EA hours		
	1	3	6	1	3	6	1	3	6	1	3	6
Section I												
Sustentacular cell necrosis	—[b]	—	—	—	—	—	—	—	—	—	—	—
Olfactory degeneration and desquamation	—	—	—	—	—	—	—	—	—	—	—	—
Epithelial folding	—	—	—	—	—	—	—	—	—	—	—	—
Section II												
Sustentacular cell necrosis	—	—	—	—	—	—	—	—	—	—	—	—
Olfactory degeneration and desquamation	—	—	—	—	—	—	—	—	—	—	—	—
Epithelial folding	—	—	—	—	—	—	—	—	—	—	—	—
Section III												
Sustentacular cell necrosis	—	—	—	—	—	—	—	2/5	3/5	—	5/5	4/5
Olfactory degeneration and desquamation	—	—	—	—	—	—	—	2/5	3/5	—	5/5	5/5
Epithelial folding	—	—	—	—	—	—	—	—	—	—	—	—
Section IV												
Sustentacular cell necrosis	—	—	—	—	—	—	—	—	3/5	—	4/5	5/5
Olfactory degeneration and desquamation	—	—	—	—	—	—	—	—	3/5	—	4/5	5/5
Epithelial folding	—	—	—	—	—	—	—	—	3/5	—	4/5	5/5
Section V												
Sustentacular cell necrosis	—	—	—	—	—	—	—	—	3/5	—	2/5	3/5
Olfactory degeneration and desquamation	—	—	—	—	—	—	—	—	—	—	2/5	2/5
Epithelial folding	—	—	—	—	—	—	—	—	—	—	1/5	2/5

[a] Anterior to posterior nasal sections I–V according to the criteria of Young, 1981. The lesions were observed only in the olfactory epithelium.
[b] No visible lesion on histopathological evaluation.

deposition equal to 1.0 represents 100% deposition of the vapor in the nasal cavity; Fig. 5). Fractional deposition data for ethyl acrylate has been reported from two laboratories using a similar experimental design (Stott and McKenna, 1984; Stott *et al.*, 1986; Morris and Frederick, 1994; Morris, 1999). Both laboratories used pretreatment with an organophosphate esterase inhibitor to demonstrate that approximately one-half the deposition of the vapor in the nasal cavity was dependent on nasal esterase activity. Estimates of the extent of enzyme inhibition *in vivo* are problematic. The CFD–PBPK simulations of enzyme inhibition of the Morris and Frederick study and the Stotta and McKenna study used estimates of inhibition of 80 and 95%, respectively. Variation in the results between the two laboratories can be attributed to experimental differences in the strain of animal used and selection and dose of esterase inhibitor that was used. In the comparisons to the experimental data, the model predicted fractional deposition within ± 0.09 of the experimental mean for all dose groups and

TABLE 2
Effects on Nonprotein Sulfhydryl Content in Various Regions of the Rat Nasal Cavity Following Acute Nose-Only Inhalation Exposure to Ethyl Acrylate Vapors

	0 h	1 h		3 h		6 h	
Tissue	0 ppm	5 ppm	25 ppm	5 ppm	25 ppm	5 ppm	25 ppm
Respiratory epithelium on the septum	100 ± 13[a]	103 ± 22	100 ± 40	92 ± 13	75 ± 8	85 ± 42	60 ± 30
Respiratory epithelium on the lateral walls of the nasal lumen	100 ± 4	94 ± 11	72 ± 4	88 ± 10	70 ± 11	88 ± 13	61 ± 8
Olfactory epithelium lining the dorsal meatus	100 ± 3	96 ± 8	65 ± 7	86 ± 5	54 ± 15	75 ± 20	41 ± 3
Olfactory epithelium on the septum	100 ± 8	98 ± 7	75 ± 4	94 ± 5	71 ± 14	82 ± 15	58 ± 10
Olfactory epithelium on the ethmoid turbinates	100 ± 45	118 ± 10	55 ± 13	92 ± 22	68 ± 17	88 ± 28	35[b] ± 13

[a] Values are means ± SD of tissues from five animals. Values are expressed as a percentage of the mean of the control values at "0 time." Data from animals exposed to a vapor concentration of 75 ppm were not used due to extensive histopathological damage to the olfactory tissue.
[b] Value is the mean of three samples. Remaining samples were lost due to experimental error.

TABLE 3
Exposure of Rat Nasal Epithelial Explants to Ethyl Acrylate *in Vitro*

EA concentration (mM)	Histopathology observations	
	Respiratory epithelium	Olfactory epithelium
0	No visible lesions	No visible lesions
0.06	No visible lesions	No visible lesions
0.3	No visible lesions	Vacuolation and nuclear swelling of sustentacular cells (3/4)[a]
0.6	No visible lesions	Vacuolation and nuclear swelling of sustentacular cells (4/4)
1.8	No visible lesions	Vacuolation and nuclear swelling of sustentacular cells (4/4)
3.6	No visible lesions	Sloughed sustentacular cells (4/4)

[a] The number of explants exhibiting the lesion out of the total examined at this exposure concentration.

was within ±0.03 of the experimental mean for six of eight dose groups (Fig. 5). This comparison of the CFD–PBPK model output to the available experimental data from two independent laboratories indicates that the model provides a reasonably good simulation of both normal and inhibited nasal uptake of this ester in an *in vivo* model.

Comparison of the Output of the CFD–PBPK Rat Model to in Vivo Data on Nonprotein Sulfhydryl Depletion

Data on variation in nonprotein sulfhydryl concentrations (primarily glutathione) associated with inhalation exposure to ethyl acrylate are available from three sources. In this study, a comparison was made of the CFD–PBPK model output to the NPSH concentration in various regions of the rat nasal cavity following acute exposure to ethyl acrylate (Table 2). Although the model predicts glutathione depletion that is time and dose dependent, the *in vivo* data tend to be considerably lower than that predicted by the model. For example, the NPSH concentration in the olfactory epithelium lining the rat dorsal meatus was decreased by 25% relative to the control tissue, but the CFD–PBPK model predicted depletion by less than 5% based solely on modeling conjugation of the unsaturated ester with gluathione. This suggests that factors in addition to conjugation of glutathione with ethyl acrylate may be influencing tissue glutathione concentrations (e.g., cellular energy status or cellular oxidation state).

In a previous study, the surgically isolated nasal cavity of rats was exposed to ethyl acrylate vapors at concentrations of 5, 25, or 88 ppm for 1 h at a unidirectional flow rate of 200 ml/min (Morris and Frederick, 1994). At the end of the exposure period, the entire nasal cavity (including all epithelial tissues and underlying connective tissue) was collected and total NPSH content measured. The mixture of tissues in the homogenate makes a quantitative comparison of NPSH concentrations to the model output difficult, but the general trend toward decreased NPSH content with increasing ethyl acrylate vapor concentrations was evident and qualitatively correlated with the model's predictions. Also consistent with the model's predictions, inhibition of esterase activity by prior treatment with an organophosphate increased the extent of NPSH depletion relative to comparable control groups.

In a third study, systemic depletion of NPSH content and lethality were evaluated following 4-h inhalation exposures to very high concentrations of ethyl acrylate (300, 500, 750, 1000, and 1500 ppm) (Silver and Murphy, 1981). Dose-dependent NPSH depletion was observed in the lungs, liver, and blood with no significant effect on the kidneys. Mortality was ob-

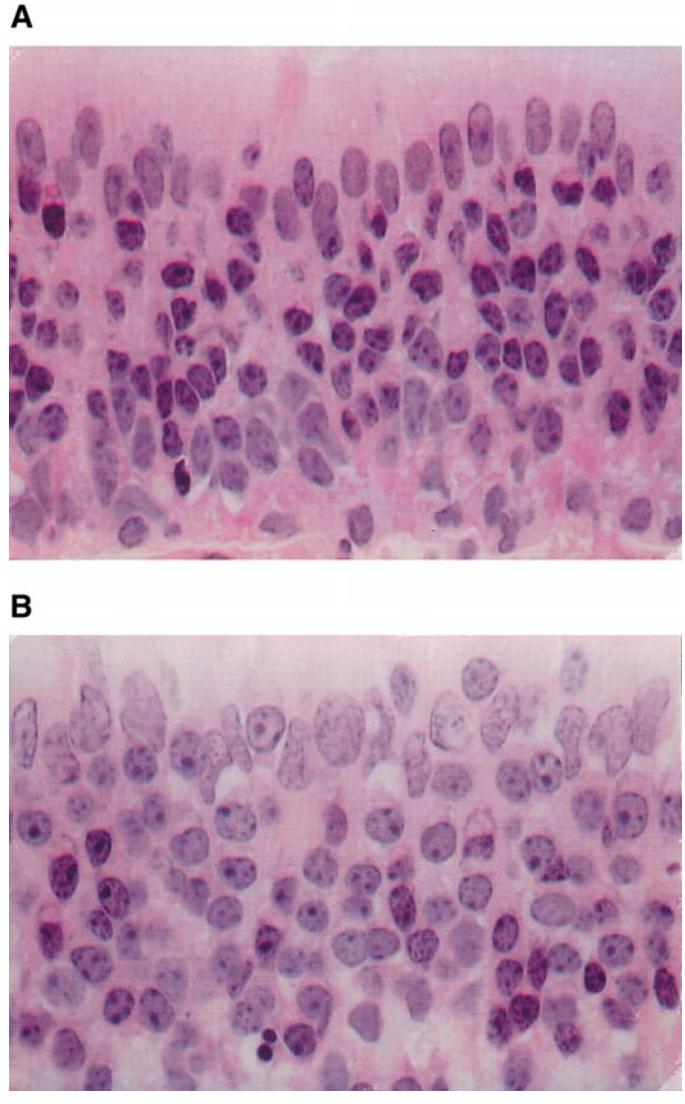

FIG. 4. Histopathology observed in the olfactory epithelium of explants of rat nasal tissue incubated with ethyl acrylate. (A) Olfactory epithelium incubated in organ culture in the absence of test compound. (B) Olfactory epithelium incubated in the presence of 0.25 mM ethyl acrylate for 2 h. Nuclear swelling and vacuolation is evident in the apical layer of sustentacular cells (top). Glycol methacrylate section with H & E staining. Magnification 400×.

TABLE 4

Effect of an Esterase Inhibitor, Paraoxon, on the Induction of Cytotoxicity in Rat Nasal Epithelial Explants by Ethyl Acrylate *in Vitro*

EA concentration (mM)	Paraoxon[a]	Histopathology observations: Respiratory epithelium	Histopathology observations: Olfactory epithelium
0	−	No visible lesions	No visible lesions
0	+	No visible lesions	No visible lesions
0.1	−	No visible lesions	No visible lesions
0.1	+	No visible lesions	No visible lesions
0.25	−	No visible lesions	Vacuolation of sustentacular cells (1/4)[b]
0.25	+	No visible lesions	No visible lesions
0.5	−	No visible lesions	Vacuolation of sustentacular cells (4/4)
0.5	+	No visible lesions	No visible lesions
1.0	−	No visible lesions	Vacuolation of sustentacular cells (4/4)
1.0	+	No visible lesions	No visible lesions

[a] +, Paraoxon concentration was 25 μM in the tissue culture media.

[b] The number of explants exhibiting the lesion out of the total examined at this exposure concentration.

served at 1500 ppm with no mortality at 1000 ppm. Both NPSH depletion and mortality were greatly increased in animals that had been treated with an organophosphate esterase inhibitor. A high incidence of mortality with quick onset was observed at 750 ppm and no mortality was observed at 500 ppm in the inhibited animals. Comparable inhalation exposure to acrylic acid at 1300 ppm resulted in no mortality and no effect of the esterase inhibitor. Simulations of very high inhalation exposures of this type with the CFD–PBPK model are challenging due to the anatomical and physiological changes (including changes in respiration rate) that are induced during near-lethal exposures. In particular, the model cannot simulate severe tissue damage and its accompanying consequences on nasal uptake. However, as a rough approximation, the CFD–PBPK model did simulate significant NPSH depletion in the lung and liver (Fig. 6) following simulated exposures in this dose range. The simulations were conducted by decreasing the simulated respiration rate by 50% from the ambient value to accommodate the RD50 data for ethyl acrylate (DeCeaurriz *et al.*, 1981). The decreases in respiration rate and tidal volume associated with inhalation exposure to high concentrations of ethyl acrylate (100–500 ppm) were confirmed by Silver *et al.* (1981), who also found that the effect was increased by prior treatment with an organophosphate esterase inhibitor.

Comparison of the Output of the CFD–PBPK Rat Model to the Histopathology Data from Nasal Explants

Histopathology data from nasal explant studies provided useful information for validation of a CFD–PBPK model for acrylic acid (Frederick *et al.*, 1998). This comparison was facilitated by the fact that acrylic acid was both causally responsible for the olfactory lesions observed in the explants as well as being the substance modeled. Dosimetry of the acrylic acid in the nasal explants could be estimated based on the concentration of the acid in the surrounding culture medium. The situation with ethyl acrylate is more complex, since acrylic acid released by metabolism of the parent ester is responsible for the olfactory cytotoxicity observed (cf. data on the nasal explant study above). Therefore, the rate of release of the acid in the explant tissue and the rate that the acid diffuses out of the explant into the surrounding culture medium (offset by the continuing accumulation of acid in the medium) will determine the steady-state concentration of the acid in the tissue. Given the uncertainty associated with the estimation of these rates, the use of the ethyl acrylate explant data for validation of the ester model is problematic. However, evaluation of the predicted acrylic acid concentration in the sustentacular cell region of the

TABLE 5

Michaelis–Menten Parameters for the Esterase-Mediated Hydrolysis of Ethyl Acrylate in Human, *Cynomolgous* **Monkey, and Rat Tissues**

Tissue	Human: No. of tissues	Human: V_{max} (μmol/ml tissue/h)	Human: K_m (μmol/ml tissue)	Monkey: No. of tissues	Monkey: V_{max} (μmol/ml tissue/h)	Monkey: K_m (μmol/ml tissue)	Rat: No. of tissues	Rat: V_{max} (μmol/ml tissue/h)	Rat: K_m (μmol/ml/tissue)
Liver	5	1070 (500–1520)	4.5 (3.2–6.0)	3	3790 (2350–5810)	3.32 (2.1–6.3)	3	1902 (1122–2838)	1.9 (1.2–2.3)
Lung	5	14.8 (5.5–29.2)	2.3 (1.3–3.3)	3	97 (58–131)	0.4 (0.3–0.5)	3	318 (306–336)	1.9 (1.2–2.6)
Kidney	2	30.9 (16.5–45.3)	5.4 (4.5–6.3)	3	127 (26–322)	1.3 (0.9–1.9)	3	210 (150–324)	15.2 (5.0–21.1)
Nasal (respiratory)	5	23.0 (18.2–25.6)	3.7 (1.9–5.2)	2	50.2 (39.0–61.4)	1.5 (1.1–1.9)	3	443 (360–500)	0.3 (0.3–0.4)
Nasal (olfactory)	4	18.1 (8.9–28.6)	2.1 (1.3–3.1)	2	66.4 (64.8–68.0)	2.4 (1.5–3.3)	3	1327 (1150–1510)	0.4 (0.3–0.5
Esophagus	3	4.6 (2.1–8.0)	10.0 (5.5–13.5)	3	109 (83–138)	3.2 (1.1–7.5)	3	15.6[a] (13.8–16.8)	3.2 (2.4–3.9)
Stomach	2	2.3 (2.2–2.4)	21.2 (14.2–28.1)	1	33.4	10.3	3	19.2[b] (18.6–19.8)	4.4 (4.0–4.8)
Blood	3	4.1 (2.2–5.9)	8.1 (3.2–12.4)	1	ND	ND	3	12 (6–18)	4.6 (1.3–7.7)

Note. Values are means with range of values observed in parentheses. ND, no detectable esterase activity.

[a] Data are for the rat forestomach.

[b] Data are for the rat glandular stomach.

TABLE 6
Nonprotein Sulfhydryl Concentration in Selected Human, *Cynomolgous* Monkey, and Rat Tissues

Tissue	Human[a] No. of tissues	Human[a] NPSH (μmol/ml tissue)	Monkey[a] No. of tissues	Monkey[a] NPSH (μmol/ml tissue)	Rat No. of tissues	Rat NPSH (μmol/ml tissue)
Liver	5	5.9 (2.8–9.9)	3	6.4 (5.1–8.0)	32	5.7 ± 0.8[b]
Lung	5	1.1 (0.4–2.1)	3	1.3 (0.6–1.9)	26	1.8 ± 0.2
Kidney	2	3.4 (2.1–4.7)	3	4.2 (3.1–5.3)	32	3.8 ± 1.3
Nasal (respiratory)	4	0.9 (0.6–1.0)	—	ND[c]	31	4.2 ± 0.6
Nasal (olfactory)	4	0.8 (0.6–1.0)	—	ND	31	3.5 ± 0.5
Esophagus	—	ND	1	0.8	26	1.5 ± 0.1[d]
Stomach	—	ND	1	1.7	26	5.7 ± 0.6[e]
Blood	2	3.5 (0.7–6.4)	1	0.4	26	1.1 ± 0.2

[a] Values are means with range of values observed in parentheses.
[b] Values are means ± SD.
[c] ND, no data because adequate tissue was not available.
[d] Tissue from the rat forestomach.
[e] Tissue from the rat glandular stomach.

most anterior olfactory compartment (the first region to exhibit cytotoxicity in an inhalation dose–response study; Table 1; also Lomax *et al.*, 1994; Frederick *et al.*, 1998) during simulation of an *in vivo* inhalation exposure to ethyl acrylate was informative. The predicted tissue concentration of acrylic acid was compared to the acrylic acid concentration that induced a cytotoxic effect in nasal tissue explants as previously described (Frederick *et al.*, 1998). The predicted acrylic acid olfactory tissue concentrations associated with breathing either 25 or 75 ppm ethyl acrylate by rats are described in Fig. 7. Acute inhalation exposure of rats in this concentration range (25–75 ppm) for 3 h induced olfactory cytotoxicity (Table 1). The figure also notes the tissue concentration of acrylic acid (0.6 mM) that resulted in a cytotoxic effect in rat olfactory tissue explants by histopathological evaluation (Frederick *et al.*, 1998). The comparison of the model predictions to the cytotoxic tissue concentration of acrylic acid is reasonably good given the approximations inherent in the model design and in the experimental conduct of the nasal explant study.

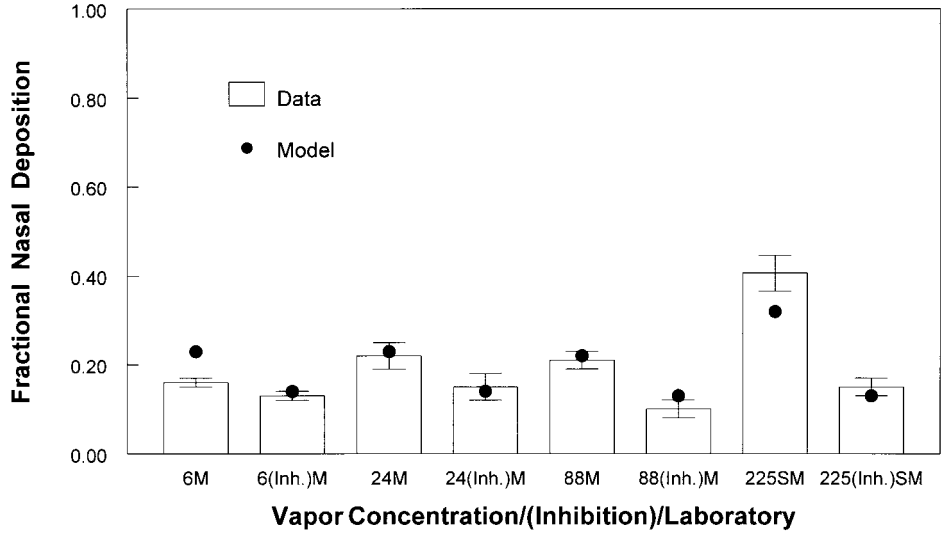

FIG. 5. Comparison of CFD–PBPK model predictions to the unidirectional rat nasal deposition data for ethyl acrylate vapor (Stott and McKenna, 1984; Stott *et al.*, 1986; Morris and Frederick, 1994) using the basic methodology described by Morris (1999). The bars represent the experimental data for the fraction of the inhaled vapor that was deposited in the rat nasal cavity. The data from the Morris and Frederick study (M) was collected at 6, 24, and 88 ppm at a flow rate of 200 ml/min with and without an organophosphate esterase inhibitor. The Stott and McKenna data (SM) were collected at 225 ppm at a flow rate of 105 ml/min. The filled circles represent the predictions of the model under the relevant exposure conditions (vapor concentration, flow rate, and with or without esterase inhibition).

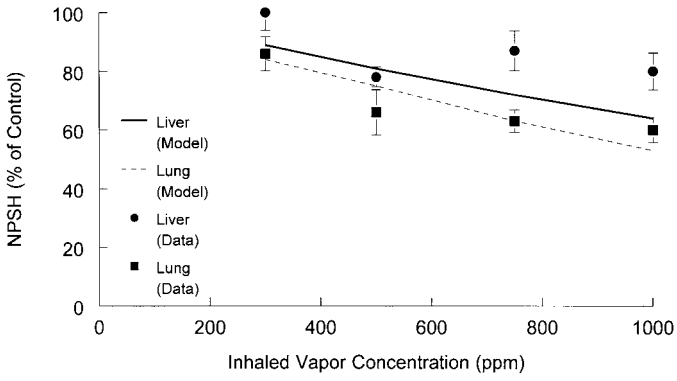

FIG. 6. Dose response for the depletion of nonprotein sulfhydryl content in the rat liver and lung following a 4-h inhalation exposure to very high concentrations of ethyl acrylate vapor. The data are from Silver *et al.* (1981). The model simulations were conducted with the minute volume decreased by 50% to accommodate respiratory depression reported at ethyl acrylate exposure concentrations in excess of 100 ppm (Silver *et al.*, 1981; DeCeaurriz *et al.*, 1981).

Interspecies Dose Comparisons from Simulations of the CFD–PBPK Model

The CFD–PBPK model can be used to estimate the tissue concentrations of acrylic acid and ethyl acrylate following a variety of simulated *in vivo* inhalation exposures. In addition, various parameter sets may be used to estimate the intraspecies range of metabolism and associated tissue concentrations that might be associated with inhalation exposure. For this discussion, three esterase parameter sets were used to describe a range of esterase activity in the human nasal cavity. One set was derived from human olfactory tissues from freshly collected autopsy samples that were evaluated for esterase activity in our laboratory (Table 5). A second set of parameters was based upon the data of Mainwaring *et al.* (2001) for human nasal biopsy tissue using a similar ester (methyl methacrylate) as a substrate (incorporated in the CFD–PBPK model as a V_{max} for respiratory and olfactory tissues that is $\frac{1}{7}$ and $\frac{1}{13}$, respectively, of the value of the comparable rat nasal tissues with the same K_m as the primate nasal tissues). A third set of parameters was based on nasal tissues collected from primates (Table 5). These parameters should be viewed as being representative of the currently available data, and additional data for the model's parameters may easily be incorporated as they become available. It should be noted that it is very difficult to obtain "good quality" human olfactory tissue due to its relatively small size and inaccessible location in the human nasal cavity.

Representative simulation results from the CFD–PBPK model for the dose responses for the olfactory tissue concentration of acrylic acid released by metabolism of ethyl acrylate are provided in Figs. 8A and 8B. The predictions are based upon simulated 1-h exposures under either resting (Fig. 8A) or light activity/working conditions (Fig. 8B) for a representative 70-kg human. Comparable curves could be generated for other exposure scenarios. Trial simulations up to 6 h indicated that steady-state nasal tissue concentrations of both the ester and acid were reached in less than 1 h. Evaluation of the simulation data indicates that the nasal tissue concentration of acrylic acid is based on the amount released from ethyl acrylate deposited in the nasal cavity as well as acrylic acid that has partitioned into nasal tissue from the blood vessels that perfuse the tissue following systemic metabolism of ethyl acrylate. Prior simulation results (Frederick *et al.*, 1992) and experimental data (Frederick *et al.*, 1992; National Toxicology Program, 1986) have indicated that ethyl acrylate has a very short half-life systemically (on the order of seconds). Although acrylic acid is also rapidly metabolized and eliminated (Black and Finch, 1995; Winter *et al.*, 1992), its systemic half-life is somewhat longer in rats (on the order of 1 h) and the model predicts distribution and metabolism of released acrylic acid to systemic tissues prior to metabolism and elimination (primarily as carbon dioxide). Under the same exposure scenario, the simulation data (Figs. 8A and 8B) indicate that human olfactory tissue would be exposed to considerably less acrylic acid (18- to 75-fold lower tissue concentrations) relative to comparable rodent olfactory tissue. The magnitude of this difference depended on the esterase dataset used for the human simulations (the primary determinate) as well as the simulated respiration rate. The model can incorporate oral breathing and greater direct exposure of the lungs and systemic tissues under working conditions. As an example, simulations were also conducted under the "light activity/working" conditions described

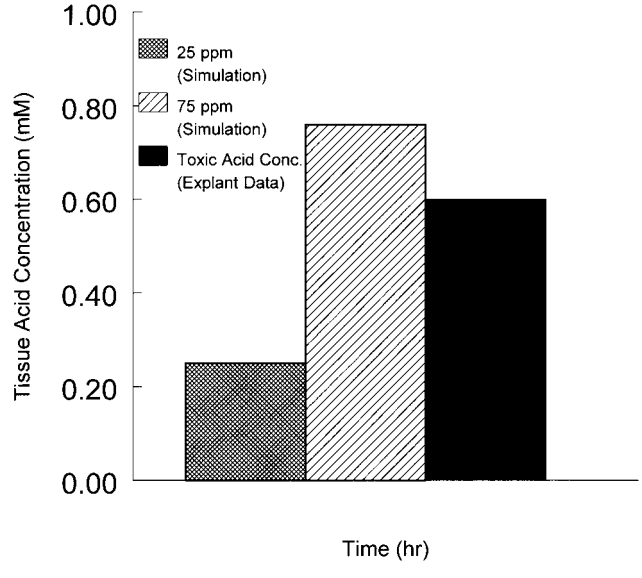

FIG. 7. A comparison of the predicted steady-state tissue concentrations of acrylic acid released by the esterase catalyzed hydrolysis of ethyl acrylate in the apical olfactory tissue layer lining the dorsal meatus. The cyclic flow simulations were conducted with simulated exposures to 25 or 75 ppm ethyl acrylate vapor for 1 h (hatched bars). A simulated 1 h exposure was sufficient to establish steady-state tissue concentrations. The solid bar is the acrylic acid concentration associated with cytotoxicity in explants of rat olfactory tissue (Frederick *et al.*, 1998).

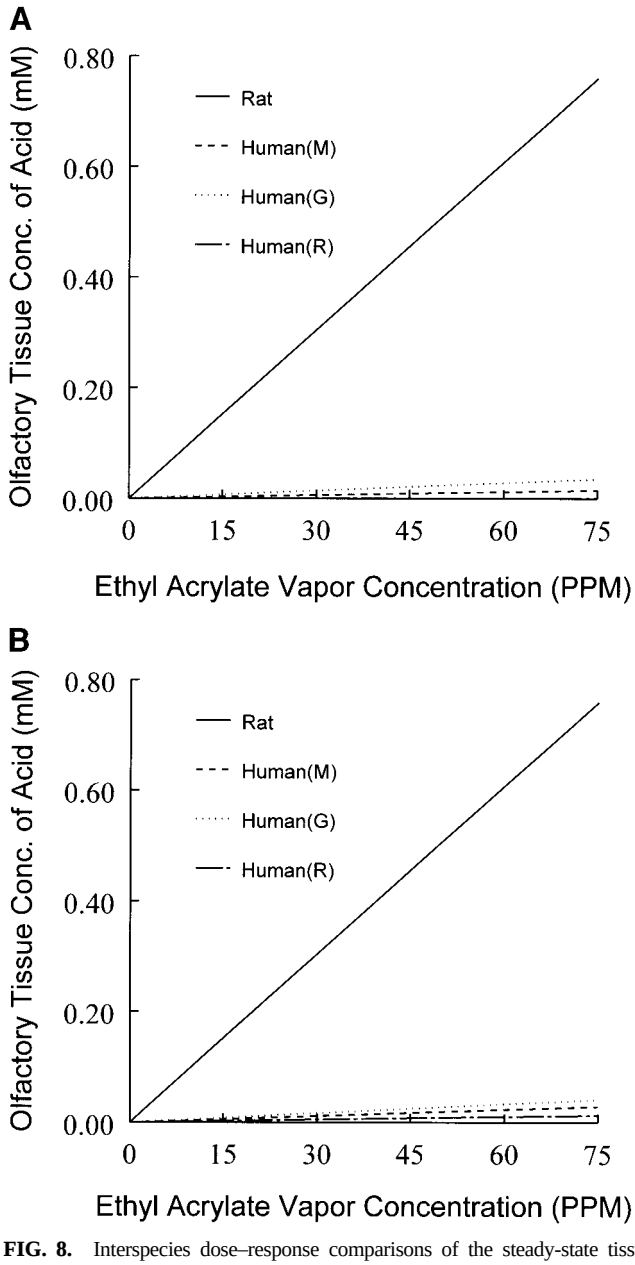

FIG. 8. Interspecies dose–response comparisons of the steady-state tissue concentration of acrylic acid that accumulates in the apical layer of olfactory tissue following inhalation exposure to ethyl acrylate. Identical cyclic flow exposure concentrations and duration (1 h) were used for the simulations for both species. The rat simulations were conducted with a simulated minute volume of 250 ml/min (respiration rate of 150 breaths/min with a tidal volume of 1.67 ml per breath). The human simulations were conducted with a simulated minute volume of 9.45 L/min (A; respiration rate of 15 breaths/min with a tidal volume of 0.63 L per breath) or 17.5 L/min (B; respiration rate of 20 breaths/min with a tidal volume of 0.875 L per breath) to simulate respiration associated with either resting or light activity, respectively. Three sets of nasal esterase Michaelis–Menten parameters were used based on the data reported in this study for primates (M), in this study for human tissues (R), and for human tissues evaluated for esterase activity with a related ester (G) (Mainwaring *et al.*, 2001).

in the legend to Fig. 8B, with a fraction of oral breathing (40%) based on the oronasal distribution data of Chadha *et al.* (1987). Simulations involving oral breathing of a fraction of the inspired air used nasal mass transport coefficients for the inspired vapor that were appropropriate for the velocity of the air passing through the nasal cavity, and they resulted in nasal olfactory tissue concentrations appropriate for the net air flow flowing through the nasal cavity. Other activity and oronasal breathing patterns can be easily accomodated. Although oral breathing provides greater exposure of the pharynx and lower respiratory tract to the inspired vapor, the available histopathology data indicate that the epithelium lining these regions is resistant to the toxic effects of acids and esters.

Applicability of the CFD–PBPK Model to Other Vapors and Esters

The model can be easily modified to accommodate the partitioning, distribution, and metabolism of other inhaled vapors. As an example, the model was parameterized to simulate the unidirectional flow deposition in the rat nasal cavity of ethyl acetate (a saturated ester) and acetone (a relatively slowly metabolized ketone that is not an esterase substrate) based on the data of Morris (1990) and Morris *et al.* (1993). The changes made to the model to accommodate these vapors were simple, i.e., set the glutathione conjugation rate to zero for the saturated ester and also set the hydrolysis rate to zero for the ketone. In both cases, the appropriate partition coefficients were provided. In the case of ethyl acetate, as a rough estimate the same Michaelis–Menten parameters as were used for ethyl acrylate were used to describe enzymatic ester hydrolysis. The comparison of the predictions of the model to the experimental data on the fractional deposition of these compounds (Fig. 9) indicates that the model structure has general applicability for a range of metabolized and nonmetabolized (or slowly metabolized) vapors. The results suggest that the V_{max} values used for the hydrolysis of ethyl acetate are too high. Refinement of the esterase parameters for ethyl acetate would probably improve the correlation of the model output with the data. Since esterase metabolism in the CFD–PBPK model is based upon Michaelis–Menten kinetics, the model can also be easily modified to accommodate other metabolic pathways with similar kinetic profiles (e.g., cytochrome P-450-mediated oxidation).

DISCUSSION

One of the most important uses of a PBPK model is to quantitatively integrate mechanistic data to provide understanding of toxic responses. This role is particularly important if the effect is based on the balance of competing rates (e.g., rate for formation of a toxic metabolite relative to the rate of its detoxification and rate of absorption relative to elimination). Obviously, many mechanistic toxicology issues are fundamentally based on the balance of competing rates. Overlaid on these kinetic processes are the underlying pharmacodynamic issues associated with tissue susceptibility to potentially toxic processes. The mechanistic toxicity issues addressed in this

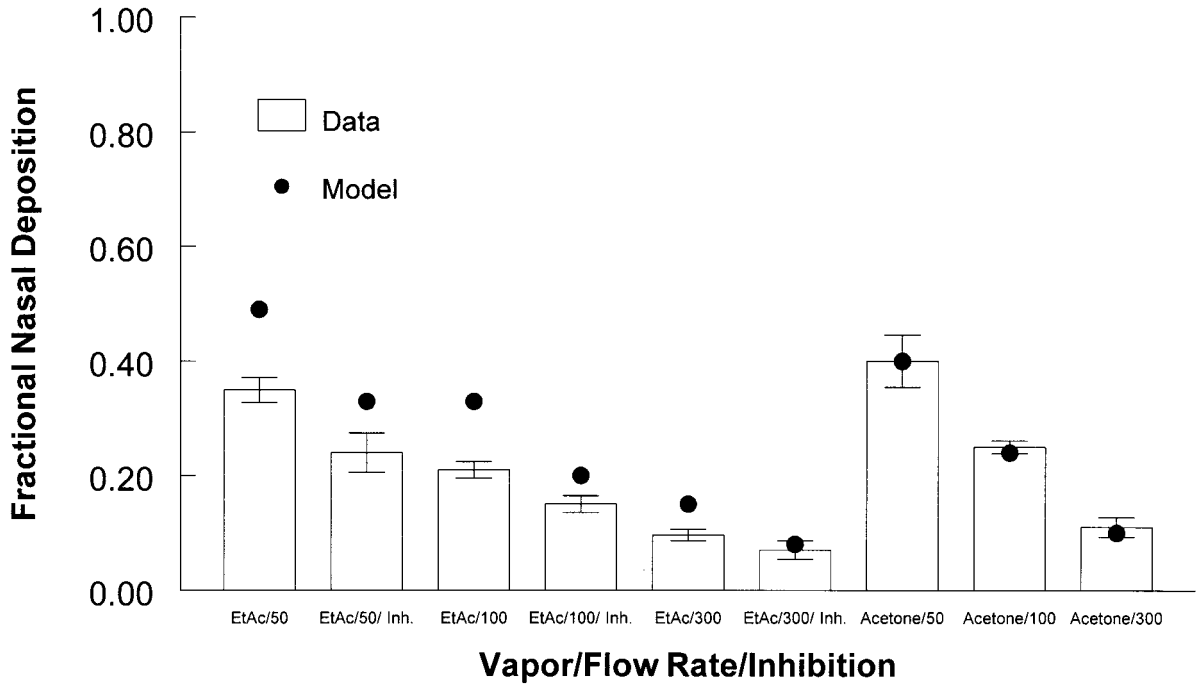

FIG. 9. Comparison of the fraction of inhaled ethyl acetate (EtAc) or acetone that is deposited in the rat nasal cavity under unidirectional flow conditions according to the methodology of Morris (1999) with the prediction of the CFD–PBPK model (round dots). The data were collected at three flow rates (50, 100, and 300 ml/min) and either with or without esterase inhibition in the case of ethyl acetate. Model simulations were conducted under the same conditions using an estimate of 80% enzyme inhibition for the inhibitor studies with ethyl acetate. For the ethyl acetate simulations, the Michaelis–Menten parameters for the esterase hydrolysis of ethyl acrylate by rat tissues were used as a rough estimate.

study incorporate all of these aspects, and the integration of this mechanistic information into a comprehensive CFD–PBPK model facilitates its use for risk assessment.

An unsaturated ester such as ethyl acrylate is typically metabolized by two major pathways: esterase-mediated hydrolysis of the ester moiety and conjugation with glutathione (which may or may not be enzyme catalyzed). Each pathway has the potential for inducing a toxic response in a susceptible tissue either from the esterase-mediated release of a toxic acid or alcohol or from depletion of tissue glutathione. The toxic responses addressed in this study are mediated by both pathways. The olfactory cytotoxicity induced in the rat nasal cavity following inhalation exposure to ethyl acrylate in the 25- to 75-ppm concentration range was mediated by release of acrylic acid based upon the nasal explant studies reported above. At much higher inhalation exposures (500–1500 ppm), lethality that was associated with severe nonprotein sulfhydryl depletion in multiple systemic tissues was observed (Silver *et al.*, 1981). Previous studies have also associated gavage dosing of high concentrations of ethyl acrylate with severe glutathione depletion and toxicity in the rat forestomach (the contact site for gavage dosing) without the significant glutathione depletion or toxicity in systemic tissues (e.g., Ghanayem 1985a,b; Frederick *et al.*, 1992).

The CFD–PBPK model described in this study uses the mechanistic information that is available from a variety of studies directly without fitting of model parameters (e.g., the metabolic data from tissue homogenates in Tables 5 and 6 is used directly). Consequently, all of the issues associated with the conduct of a study in the laboratory that provides the parameters (e.g., animal husbandry, tissue collection, and methodology for conducting *in vitro* studies) can contribute to the quality of the model's output. Similarly, a variety of assumptions are inherent in the model design that can influence the behavior of the model (e.g., the use of well-stirred air and tissue compartments, estimates of tissue blood flow, and estimates of enzyme inhibition *in vivo* in inhibitor studies; discussed in detail in Bush *et al.*, 1998 and Frederick *et al.*, 1998). As previously elaborated (e.g., Conolly and Andersen, 1991), the use of a biologically based model allows an explicit evaluation of the sensitivity of the model output relative to variation in model parameters, and an extensive sensitivity analysis was conducted for the CFD–PBPK for acrylic acid that formed the basis for the ester model (Andersen *et al.*, 2000). In this study, the comparison of the model output to experimental data requires an evaluation of the uncertainty associated with the model design relative to the variability of the experimental data from multiple laboratories for several vapors. For example, is a discrepancy in the range of 0.07–0.09 in the model's prediction of the fractional deposition of ethyl acrylate relative to experimental data in three of eight comparisons significant (Fig. 5; deposition data from two laboratories)? Or is this much

variation inherent in the experimental variability and in unexplained differences between laboratories? In our opinion, given the fact that the model's parameters were gathered in many laboratories and used without fitting, and the experimental data used to evaluate the model output also came from several laboratories at different times, it is remarkable that the model's output is as accurate as it is in correlating with the experimental observations. The consistency and adequacy of this correlation provides confidence that the model structure is robust and suitable as a useful tool for risk assessment and the establishment of human exposure limits.

Additional confidence is provided by the fact that the model is based upon the structure of an acid inhalation model that was also extensively evaluated (Bush *et al.*, 1998; Frederick *et al.*, 1998). The acid inhalation model was subjected to extensive sensitivity and uncertainty analysis and found to be a robust and useful tool for risk assessment and for the establishment of human inhalation exposure limits (Andersen *et al.*, 2000). To modify the acid inhalation model to describe inhalation exposure to an ester, the description of acid-specific processes (e.g., a description of ionization of the acid, and pH and buffer capacity of mucus and tissue) was deleted. Instead, simulation language was added to describe the second-order rate of conjugation of an unsaturated ester with glutathione and to describe the normal rate of glutathione synthesis and turnover in tissues. In addition, simulation language was added to describe the Michaelis–Menten hydrolysis of esters by tissue esterases, and a nested metabolite model describing the Michaelis–Menten metabolism of the released acid metabolite was added. The nested acid PBPK metabolite model was constructed similarly to previous PBPK models that have described the metabolic release of other acidic metabolites (e.g., Gargas *et al.*, 2000a,b; Hays *et al.*, 2000). The descriptions of the glutathione conjugation, synthesis, and turnover and the description of metabolism by tissue esterases were derived from a previously published and extensively evaluated oral PBPK model for ethyl acrylate (Frederick *et al.*, 1992). The consistent use of the same model components with good correlations to the available experimental data across multiple studies suggests that the basic structure of the model is sound. In addition, the observation that the rat nasal deposition data for a saturated ester, ethyl acetate, could be replicated by simply "turning off" the rate of glutathione conjugation is supportive. The general utility of the model for other vapors is demonstrated by its reasonable performance in replicating both the ethyl acetate and the acetone nasal deposition data by simply substituting the appropriate substance-specific partition coefficients and making the appropriate changes for the rates of glutathione conjugation and esterase activity for each substance. The use of Michaelis–Menten kinetics to describe tissue esterase activity means that the substitution of the appropriate constants and enzyme distributions for other metabolic activities (e.g., cytochrome P450-mediated oxidations) would be straightforward. Furthermore, the incorporation of systemic circulation in the nasal model allows the evaluation of metabolism and tissue dosimetry of substances that induce nasal toxicity following oral dosing (e.g., Wetmore *et al.*, 1999 and references cited therein).

The tissue dose predictions of the CFD–PBPK ester model provide an interesting comparison to the tissue dose predictions of the previously published CFD–PBPK acid model (Bush *et al.*, 1998; Frederick *et al.*, 1998). Notably, the acid model predicts very high uptake in the rat nasal cavity (nearly 100%) that would only be diminished somewhat by accumulation of acid in the mucus layer with an accompanying significant decrease in the mucus pH. The model predictions were supported by unidirectional flow nasal uptake data in the rat (Morris and Frederick, 1994). The limited perfusion of the nasal cavity slows the distribution of deposited vapors systemically and effectively limits the systemic dose during relatively short exposure periods. In contrast, the CFD–PBPK ester model predicts much lower uptake in the rat nasal cavity (approximately 20% of the inhaled vapor in unidirectional flow simulations), which is consistent with the experimental data (Morris and Frederick, 1994). The fact that the nasal fractional deposition of the ester is much lower means that the entire nasal cavity is exposed to a much more uniform concentration of the vapor in the gas phase and much more of the vapor penetrates the nasal cavity to expose the conducting airways and tissue of the lower respiratory tract. Under these circumstances, local metabolism of the absorbed vapor by tissue esterases and glutathione conjugation becomes more important in determining the local steady-state tissue concentration than the distribution of nasal air flow. Similarly, the penetration of the vapor to the conducting airways and lower respiratory tract facilitates the systemic distribution and metabolism of the vapor and its metabolites and increases systemic exposure. The increased systemic exposure also facilitates increases in nasal tissue concentrations of the vapor and its metabolites via recirculation and partitioning from the blood perfusing the nasal cavity. Although this increase in systemic exposure could be viewed as adverse from a risk assessment perspective, the chronic inhalation studies that have been conducted with ethyl acrylate provide confidence that no toxic effects are induced in systemic organs during inhalation exposure (Miller *et al.*, 1985). The chronic bioassay did provide evidence of olfactory cytotoxicity and replacement of damaged olfactory epithelium with resistant respiratory epithelium in the nasal cavity at high vapor concentrations of ethyl acrylate.

The most practical application of a PBPK model is to use the model for interspecies dose extrapolation. In this case, the CFD–PBPK model predicts that the steady-state released acid concentration in the most susceptible region of the rat nasal cavity is at least 18 times higher than in the most comparable region of the human nasal cavity under the same exposure conditions. Although nasal tissue dosimetry is based on species-specific air patterns, mass transfer coefficients, and metabolism, evaluation of the model performance indicates that

the primary basis for this difference is that the human nasal cavity has much less esterase activity than the rat nasal cavity. The confidence in the human esterase data is increased by the fact that the hydrolysis rates for tissues in the monkey nasal cavity were not significantly higher than the human values. This conclusion has important ramifications, because it suggests that interindividual differences in air flow patterns based on differences in nasal anatomy may have relatively little impact on the accumulation of the toxic acid in nasal tissues relative to the large interspecies differences in nasal esterase activity.

Given the lack of systemic toxicity for ethyl acrylate in the inhalation chronic bioassay (Miller *et al.*, 1985), the focus of the interspecies dose comparison for the most susceptible tissue is the olfactory region of the nasal cavity. Olfactory tissue in rodents and humans is similar in structure and there is no evidence available that indicates that there is a significant difference between species in tissue susceptibility to acids or esters. Since the chronic inhalation study provided no evidence of toxicity in the rat or mouse nasal cavity (or any systemic tissue) following chronic exposure to 5 ppm ethyl acrylate vapor, and the CFD–PBPK modeling exercises indicate that human nasal tissue dosimetry is at least 18-fold lower than comparable animal tissue, it may be concluded that human inhalation exposure in the the dose range of current occupational exposure limts (2–5 ppm) does not appear to have a significant risk of inducing toxicity.

APPENDIX

As described under Materials and Methods, the model was based upon the basic model structure of a previously published CFD–PBPK model for acrylic acid (Frederick *et al.*, 1998). The description of gas phase mass transport and the rate equations describing mass transport within tissues are the same. The anatomical and physiological parameters are unchanged. Appropriate changes were made to accommodate a description of metabolism for an unsaturated organic ester. For the ester model, the ionization components of the acid model were deleted and the following components were added: partition coefficients for ethyl acrylate, a Michaelis–Menten description of tissue esterase activity for both the rat and human, a description of steady-state tissue glutathione concentration and the second-order conjugation of the unsaturated ester by glutathione, a nested PBPK description of the metabolism and distribution of the acid released by the esterase, a kidney compartment to describe renal metabolism of the released acid since the kidneys are the dominant metabolism site (Black and Finch, 1995), and a description of oral breathing that bypasses the nasal cavity to simulate the human breathing pattern for simulations of working conditions (Chadha *et al.*, 1987). The rate equations describing esterase metabolism, glutathione conjugation, and tissue glutathione concentration (based on the relative rates of glutathione synthesis and turnover) are described in Appendix I of Frederick *et al.* (1992). Esterase activity in the respiratory epithelium of the dorsal meatus (a nontarget tissue) was modeled based on first-order kinetics to accommodate aberrant model performance traced to a problem in the underlying simulation language. This use of this approximation was supported by predicted tissue concentrations, which were much less than the K_m in the exposure range of concern for risk assessment. A description of glutathione "overshoot" following severe glutathione depletion as was previously described for gastric tissues following gavage dosing (Frederick *et al.*, 1992) was not included in this model. Metabolism of the released acrylic acid was described by Michaelis–Menten kinetics in the nasal epithelial tissue layers and in systemic organs with metabolic constants based on Finch and Frederick (1992) and Black and Finch (1995). The structure of the nested acid metabolite PBPK model was based on the structures of prior PBPK models that described the metabolic release of toxicologically significant metabolites (e.g., Gargas *et al.*, 2000a,b; Hays *et al.*, 2000 for acid metabolite examples) and on the prior CFD–PBPK model for acrylic acid (Frederick *et al.*, 1998; substituting metabolic release in tissues for inhalation exposure). The rate equations and model parameters that are specific to the ethyl acrylate CFD–PBPK model are listed below.

Nasal epithelial phases. The description of diffusion of the vapor in the nasal epithelial layers differs from the previous acrylic acid model by substituting a description of esterase activity and glutathione conjugation for the previous description of acid metabolism. For Fick's Law diffusion between adjacent tissue compartments with a partition coefficient approximately equal to unity between compartments:

$$V_i dC_i/dt = D_{epi}/l_{i-i-1}S_c(C_{i-i-1} - C_i) - D_{epi}/l_{i-i+1}S_c(C_i - C_{i-i+1}) - V_i V_{maxt} C_i/(K_{mt} + C_i) - V_i K_{gsht} C_i G_i \quad (1)$$

where

V_i = volume of the ith tissue compartment (cm^3); assume 1 ml $\cong$ 1 cm^3

C_i, C_{i-i-1}, C_{i-i+1} = vapor concentrations in the ith tissue compartment and the compartments above and below it (μmol/cm^3)

D_{epi} = diffusivity of the compound in the epithelial phase (cm^2/h)

l_{i-i-1}, l_{I-i+1} = lengths of the diffusion paths between midpoints of epithelial layers (cm)

V_{maxt} = Michaelis–Menten V_{max} parameter for tissue esterase metabolism (μmol ml^{-1} h^{-1})

K_{mt} = Michaelis–Menten k_m parameter for tissue esterase metabolism (μmol/cm^3)

K_{gsht} = second-order rate constant for conjugation with glutathione (cm^3 h^{-1} μmol^{-1})

G_i = glutathione concentration (μmol/cm^3)

Similarly, for the formation, metabolism, and transport of acrylic acid in a tissue layer:

$$V_i dC_{ai}/dt = D_{epi}/l_{i-i-1}S_c(C_{ai-ai-1} - C_{ai}) - D_{epi}/l_{i-i+1}S_c(C_{ai} - C_{ai-ai+1}) - V_i V_{amaxt}C_{ai}/(K_{amt} + C_{ai}) \quad (2)$$

where

C_{ai}, $C_{ai-ai-1}$, $C_{ai-ai+1}$ = acid concentration in the ith tissue compartment and the compartments above and below it (μmol/cm^3)

V_{amaxt} = Michaelis–Menten V_{max} parameter for tissue acid metabolism (μmol ml^{-1} h^{-1})

K_{amt} = Michaelis–Menten k_m parameter for tissue acid metabolism (μmol/cm^3)

Nasal blood-exchange region. Assuming approximately equal diffusion coefficients in the epithelial layer adjacent to the blood exchange region and in the blood exchange region and a partition coefficient between these regions of approximately one:

$$V_{ex}dC_{ex}/dt = D_{epi}/l_{epi-ex}S_c(C_{epi} - C_{ex}) + Q_{blood}(C_{art} - C_{ex}) - V_{ex}V_{maxt}C_{exi}/(K_{mt} + C_{ex}) - V_{ex}K_{gsht}C_{ex}G_{ex} \quad (3)$$

where

V_{ex} = volume of tissue compartment in blood exchange region (cm^3)

C_{epi} = concentration in the tissue compartment above the blood-exchange region (μmol/cm^3)

C_{ex} = concentration in the blood exchange region (μmol/cm^3)

C_{art} = concentration in the arterial blood entering the blood-exchange region (μmol/cm^3)

l_{epi-ex} = length of the diffusion path from midpoint of epithelial layer adjacent to the blood exchange region to the midpoint of the blood exchange region (cm)

V_{maxt} = Michaelis–Menten V_{max} parameter for tissue esterase metabolism (μmol ml^{-1} h^{-1})

K_{mt} = Michaelis–Menten k_m parameter for tissue esterase metabolism (μmol/cm^3)

K_{gsht} = second-order rate constant for conjugation with glutathione (cm^3 h^{-1} μmol^{-1})

G_{ex} = glutathione concentration (μmol/cm^3)

In addition to the parameter values listed in Tables 4 and 5 and those cited from the previously published oral PBPK for model for ethyl acrylate (Frederick *et al.*, 1992) and the CFD–PBPK model for acrylic acid (Bush *et al.*, 1998; Frederick *et al.*, 1998; Andersen *et al.*, 2000), the remaining model parameters that were used and their source is cited below.

The tissue:blood partition coefficients for ethyl acrylate that were used in the CFD–PBPK model were different from those originally reported in Frederick *et al.* (1992), since residual blood esterase activity was subsequently detected using the methodology that was used for the original determinations of the blood:air partition coefficient (see corrective note in Frederick *et al.*, 1994a). The revised blood:air partition coefficient for ethyl acrylate that was determined with effective blood esterase inhibition and cited in Frederick *et al.* (1994a) was 86 ± 21. Recalculation of the remaining tissue:blood partition coefficients from Frederick *et al.* (1992) based on the revised value for the blood gave the following parameter values that were used in the CFD–PBPK model:

Lung:blood partition coefficient = 1.2
Liver:blood partition coefficient = 1.7
Kidney:blood partition coefficient = 1.1
Poorly perfused:blood partition coefficient = 2.0 (based on the determination for muscle)
Richly perfused:blood partition coefficient = 1.7
Nasal tissue:blood partition coefficient = 1.7 (value for richly perfused tissue)
Mucus:air partition coefficient = 86.0 (estimate based on blood:air)
Blood:air partition coefficient = 86.0
Mucus:epithelium partition coefficient = 1.0 (estimate)

The partition coefficients used for the acrylic acid released by esterase activity in the nested metabolite model were the same as those published in Frederick *et al.* (1998).

The Michaelis–Menten constants used for the metabolism of acrylic acid were based on *in vitro* assays with rat tissues conducted by Finch and Frederick (1992) and Black and Finch (1995):

K_m for all tissues = 0.5 μmol/ml
V_{max} for respiratory epithelium = 4.0 μmol/ml/h
V_{max} for olfactory epithelium = 4.0 μmol/ml/h
V_{max} for liver = 16.9 μmol/ml/h
V_{max} for kidney = 31.3 μmol/ml/h
V_{max} for lung = 4.0 μmol/ml/h
V_{max} for richly perfused tissues = 4.0 μmol/ml/h
V_{max} for poorly perfused tissues = 1.0 μmol/ml/h

Additional CFD simulations were conducted on the CFD model of the human nasal cavity at a flow rate of 35 L/min to approximate the nasal flow dynamics of a human in a light activity work pattern with a 50-W work load (Chadha *et al.*, 1987). These mass transport values were used for simulations of an adult human under a light activity work load. The simulations were conducted with a gas phase diffusivity of 0.1 cm^2/s. Regional flow is the fraction of total air flow entering each region of the nasal cavity (dimensionless). In the olfactory region, there was a significant loss of air flow between the

anterior and posterior faces of the region. This loss of air flow is accounted for in the posterior ventral respiratory region of the model. Regional flow (dimensionless) Vestibule 1.0 DM respiratory entering region = 0.06 DM olfactory entering region = 0.08 DM olfactory exiting region = 0.03 Anterior ventral respiratory entering region = 0.94 Posterior ventral respiratory entering region = 0.92 Posterior ventral respiratory exiting region = 0.97 Pharynx 1.0 Regional gas phase mass transport coefficients (cm/s) Vestibule 4.35 DM respiratory 1.26 DM olfactory 11.52 Anterior ventral respiratory 5.32 Posterior ventral respiratory 4.66 Pharynx 3.23

ACKNOWLEDGMENTS

This model was based upon the theoretical framework for describing deposition of vapors in the nasal cavity developed in collaboration with Dr. James S. Ultman and Michele L. Bush of the Physiological Transport Studies Laboratory of Pennsylvania State University. Dr. Melvin Andersen (Colorado State University) provided thoughtful insight into the deposition of vapors in the nasal cavity and the pharmacokinetic clearance of compounds from the systemic circulation by tissues. Dr. Deborah Gillette provided additional histopathological evaluation for some of the nasal explant studies. Mr. John R. Udinsky provided technical support for much of the *in vitro* biochemical analysis. These studies were supported by the Basic Acrylic Monomer Manufacturers and Rohm and Haas Company.

REFERENCES

Aceto, A., Sacchetta, P., Dragani, B., Bucciarelli, T., Angelucci, S., Longo, V., Gervasi, G. P., Martini, F., and Diilio, C. (1993). Glutathione transferase isoenzymes in olfactory and respiratory epithelium of cattle. *Biochem. Pharmacol.* **46,** 2127–2133.

Andersen, M. E., Sarangapani, R., Gentry, R., Clewell, H., Covington, T., and Frederick, C. B. (2000). Application of a hybrid CFD–PBPK nasal dosimetry model in an inhalation risk assessment: An example with acrylic acid. *Toxicol. Sci.* **57,** 312–325.

Black, K. A., and Finch, L. (1995). Acrylic acid oxidation and tissue-to-blood partition coefficients in rat tissues. *Toxicol. Lett.* **78,** 73–78.

Bogdanffy, M. S., Randall, H. W., and Morgan, K. T. (1987). Biochemical quantitation and histochemical localization of carboxylesterase in the nasal passages of the Fischer-344 rat and B6C3F1 mouse. *Toxicol. Appl. Pharmacol.* **88,** 183–194.

Bogdanffy, M. S., Sarangapani, R., Kimbell, J. S., Frame, S. R., and Plowchalk, D. R. (1998). Analysis of vinyl acetate metabolism in rat and human nasal tissues by an in vitro gas uptake technique. *Toxicol. Sci.* **46,** 235–246.

Bush, M. L., Frederick, C. B., Kimbell, J. S., and Ultman, J. S. (1998). A CFD–PBPK hybrid model for simulating gas and vapor uptake in the rat nose. *Toxicol. Appl. Pharmacol.* **150,** 133–145.

Chadha, T. S., Birch, S., and Sackner, M. A. (1987). Oronasal distribution of ventilation during exercise in normal subjects and patients with asthma and rhinitis. *Chest* **92,** 1037–1041.

Conolly, R. B., and Andersen, M. E. (1991). Biologically based pharmacokinetic models: Tools for toxicological research and risk assessment. *Annu. Rev. Pharmacol. Toxicol.* **31,** 503–523.

Dahl, A. R., Miller, S. C., and Petridou-Fischer, J. (1987). Carboxylesterases in the respiratory tracts of rabbits, rats, and Syrian hamsters. *Toxicol. Lett.* **36,** 129–136.

DeCeaurriz, J. C., Mieillino, J. C., Bonnet, P., and Guenier, J. P. (1981). Ethyl acrylate: Sensory irritation caused by various industrial airborne chemicals (22 sensory irritants). *Toxicol. Lett.* **9,** 137–144.

Finch, L., and Frederick, C. B. (1992). Rate and route of oxidation of acrylic acid to carbon dioxide in rat liver. *Fundam. Appl. Toxicol.* **19,** 498–504.

Frederick, C. B., Potter, D. W., Chang-Mateu, M. I., and Andersen, M. E. (1992). A physiologically based pharmacokinetic and pharmacodynamic model to describe oral dosing of rats with ethyl acrylate and its implications for risk assessment. *Toxicol. Appl. Pharmacol.* **114,** 246–260.

Frederick, C. B., Morris, J. B., Kimbell, J. S., Morgan, K. T., and Scherer, P. T. (1994a). Comparison of four biologically based dosimetry models for the deposition of rapidly metabolized vapors in the rodent nasal cavity. *Inhal. Toxicol.* **6**(Suppl.), 135–157.

Frederick, C. B., Udinsky, J. R., and Finch, L. (1994b). The regional hydrolysis of ethyl acrylate to acrylic acid in the rat nasal cavity. *Toxicol. Lett.* **70,** 49–56.

Frederick, C. B., Bush, M. L., Lomax, L. G., Black, K. A., Finch, L., Kimbell, J. S., Morgan, K. T., Subramaniam, R. P., Morris, J. B., and Ultman, J. S. (1998). Application of a hybrid computational fluid dynamics and physiologically based inhalation model for interspecies dosimetry extrapolation of acidic vapors in the upper airways. *Toxicol. Appl. Pharmacol.* **152,** 211–231.

Fregosi, R. F., and Lansing, R. W. (1995). Neural drive to nasal dilator muscles: Influence of exercise intensity and oronasal flow partitioning. *J. Appl. Physiol.* **79,** 1330–1337.

Gargas, M. L., Tyler, T. R., Sweeney, L. M., Corley, R. A., Weitz, K. K., Mast, T. J., Paustenbach, D. J., and Hays, S. M. (2000a). A toxicokinetic study of inhaled ethylene glycol monomethyl ether (2-ME) and validation of a physiologically based pharmacokinetic model for the pregnant rat and human. *Toxicol. Appl. Pharmacol.* **165,** 53–62.

Gargas, M. L., Tyler, T. R., Sweeney, L. M., Corley, R. A., Weitz, K. K., Mast, T. J., Paustenbach, D. J., and Hays, S. M (2000b). A toxicokinetic study of inhaled ethylene glycol ethyl ether acetate and validation of a physiologically based pharmacokinetic model for rat and human. *Toxicol. Appl. Pharmacol.* **165,** 63–73.

Ghanayem, B. I., Maronpot, R. R., and Matthews, H. B. (1985a). Ethyl acrylate induced gastric toxicity. I. Effect of single and repetitive dosing. *Toxicol. Appl. Pharmacol.* **80,** 323–335.

Ghanayem, B. I., Maronpot, R. R., and Matthews, H. B. (1985b). Ethyl acrylate-induced gastric toxicity. II. Structure–toxicity relationships and mechanism. *Toxicol. Appl. Pharmacol.* **80,** 336–344.

Gross, E. A., Swenberg, J. A., Fields, S., and Popp, J. A. (1982). Comparative morphometry of the nasal cavity in rats and mice. *J. Anat.* **135,** 83–88.

Hays, S. M., Elswick, B. A., Blumenthal, G. M., Welsch, F., Conolly, R. B., and Gargas, M. L. (2000). Development of a physiologically based pharmacokinetic model of 2-methoxyethanol and 2-methoxyacetic acid disposition in pregnant rats. *Toxicol. Appl. Pharmacol.* **163,** 67–74.

Hext, P. M., Pinto, P. J., and Gaskell, B. A. (2001). Methyl methacrylate toxicity in rat nasal epithelium: Investigation of the time course of lesion development and recovery from short term vapour inhalation. *Toxicology* **156**, 119–128.

James, D. S., Lambert, W. E., Mermier, C. M., Stidley, C. A., Chick, T. W., and Samet, J. M. (1997). Oronasal distribution of ventilation at different ages. *Arch. Environ. Health* **52,** 118–123.

Keenan, C. M., Kelly, D. P., and Bogdanffy, M. S. (1990). Degeneration and recovery of rat olfactory epithelium following inhalation of dibasic esters. *Fundam. Appl. Toxicol.* **15,** 381–393.

Keyhani, K., Scherer, P. W., and Mozell, M. M. (1995). Numerical simulation of airflow in the human nasal cavity. *J. Biomed. Engr.* **117,** 429–442.

Kimbell, J. S., Gross, E. A., Joyner, D. R., Godo, M. N., and Morgan, K. T. (1993). Application of computational fluid dynamics to regional dosimetry of inhaled chemicals in the upper respiratory tract of the rat. *Toxicol. Appl. Pharmacol.* **121,** 253–263.

Kimbell, J. S., Gross, E. A., Richardson, R. B., Conolly, R. B., and Morgan, K. T. (1997). Correlation of regional formaldehyde flux predictions with the

distribution of formaldehyde-induced squamous metaplasia in F344 rat nasal passages. *Mutat. Res.* **380,** 143–154.

Lang, J. (1989). *Clinical Anatomy of the Nose, Nasal Cavity, and Paranasal Sinuses*. Thieme, Stuttgart.

Lewis, J. L., Nikula, K. J., Novak, R., and Dahl, A. R. (1994). Comparative localization of carboxylesterase in F344 rat, beagle dog, and human nasal tissue. *Anat. Rec.* **239,** 55–64.

Lomax, L. G., Brown, D. W., and Frederick, C. B. (1994). Regional histopathology of the mouse nasal cavity following two weeks of exposure to acrylic acid for either 6 or 22 hours per day. *Inhal. Toxicol.* **6**(Suppl.), 445–449.

Mainwaring, G., Foster, J. R., Lund, V., and Green, T. (2001). Methyl methacrylate toxicity in rat nasal epithelium: Studies of the mechanism of action and comparisons between species. *Toxicology* **158**, 109–118.

Mery, S., Gross, E. A., Joyner, D. R., Godo, M., and Morgan, K. T. (1994). Nasal diagrams: A tool for recording the distribution of nasal lesions in rats and mice. *Toxicol. Pathol.* **22,** 353–372.

Miller, R. R., Ayres, J. A., Jersey, G. C., and McKenna, M. J. (1981). Inhalation toxicity of acrylic acid. *Fundam. Appl. Toxicol.* **1,** 271–277.

Miller, R. R., Young, J. T., Kociba, R. J., Keyes, D. G., Bodner, K. M., Calhoun, L. L., and Ayres, J. A. (1985). Chronic toxicity and oncogenicity bioassay of inhaled ethyl acrylate in Fischer 344 rats and B6C3F1 mice. *Drug Chem. Toxicol.* **8,** 1–42.

Morgan, K. T., and Monticello, T. M. (1990). Airflow, gas deposition, and lesion distribution in the nasal passages. *Environ. Health Perspect.* **85,** 209–218.

Morris, J. B. (1990). First-pass metabolism of inspired ethyl acetate in the upper respiratory tracts of the F344 rat and Syrian hamster. *Toxicol. Appl. Pharmacol.* **102,** 331–345.

Morris, J. B., Hassett, D. N., and Blanchard, K. T. (1993). A physiologically based pharmacokinetic model for nasal uptake and metabolism of nonreactive vapors. *Toxicol. Appl. Pharmacol.* **123,** 120–129.

Morris, J. B., and Frederick, C. B. (1994). Upper respiratory tract uptake of acrylate ester and acid vapors. *Inhal. Toxicol.* **7,** 557–574.

Morris, J. B. (1999). A method for measuring upper respiratory tract vapor uptake and its applicability to quantitative inhalation risk assessment. *Inhal. Toxicol.* **11,** 943–965.

National Toxicology Program (1986). *Carcinogenesis Bioassay of Ethyl Acrylate.* Technical Report Series 259, Publication (NIH) 82-2515. U. S. Department of Health and Human Services, Public Health Service, National Institutes of Health, Research Triangle Park, N. C.

National Toxicology Program (1992). *Toxicity Studies of Formic Acid Administered by Inhalation for F344/N Rats and B6C3F1 Mice.* NTP Tech. Report, NIH Publication 92-3342. U. S. Dept. of Health and Human Services, Public Health Service, National Institutes of Health, Research Triangle Park, N. C.

Niinimaa, V., Cole, P., Mintz, S., and Shephard, R. J. (1980). The switching point from nasal to oronasal breathing. *Respir. Physiol.* **42,** 61–71.

Niinimaa, V., Cole, P., Mintz, S., and Shephard, R. J. (1981). Oronasal distribution of respiratory airflow. *Respir. Physiol.* **43,** 69–75.

Olson, M. J., Martin, J. L., LaRosa, A. C., Brady, A. N., and Pohl, L. R. (1993). Immunohistochemical localization of carboxylesterase in the nasal mucosa of rats. *J. Histochem. Cytochem.* **41,** 307–311.

Potter, D. W., and Tran, T.-B. (1992). Rates of ethyl acrylate binding to glutathione and protein. *Toxicol. Lett.* **62,** 275–285.

Potter, D. W., and Tran, T.-B. (1993). Apparent rates of glutathione turnover in rat tissues. *Toxicol. Appl. Pharmacol.* **120,** 186–192.

Potter, D. W., Finch, L., and Udinsky, J. R. (1995). Glutathione content and turnover in rat nasal epithelia. *Toxicol. Appl. Pharmacol.* **135,** 185–191.

Silver, E. H., and Murphy, S. D. (1981). Potentiation of acrylate ester toxicity by prior treatment with the carboxylesterase inhibitor triorthotolyl phosphate (TOTP). *Toxicol. Appl. Pharmacol.* **57,** 208–219.

Silver, E. H., Leith, D. E., and Murphy, S. D. (1981). Potentiation by triorthotolyl phosphate of acrylate ester-induced alterations in respiration. *Toxicology* **22,** 193–203.

Stott, W. T., and McKenna, M. J. (1984). The comparative absorption and excretion of chemical vapors by the upper, lower, and intact respiratory tract of rats. *Fundam. Appl. Toxicol.* **4,** 594–602.

Stott, W. T., Ramsey, J. C., and McKenna, M. J. (1986). Absorption of chemical vapors by the upper respiratory tract of rats. In *Toxicology of the Nasal Passages* (C. S. Barrow, Ed.), pp. 191–210. Hemisphere, Washington.

Subramaniam, R., Richardson, R. B., Morgan, K. T., Kepler, G., Kimbell, J. S., and Guilmette, R. A. (1998). Computational fluid dynamics simulations of inspiratory airflow in the human nose and nasopharynx. *Inhal. Toxicol.* **10,** 91–120.

Trela, B. A., and Bogdanffy, M. S. (1991). Cytotoxicity of dibasic esters (DBE) metabolites in rat nasal explants. *Toxicol. Appl. Pharmacol.* **110,** 259–267.

Wetmore, B. A., Mitchell, A. D., Meyer, S. A., and Genter, M. B. (1999). Evidence for site-specific bioactivation of alachlor in the olfactory mucosa of the Long–Evans rat. *Toxicol. Sci.* **49,** 202–212.

Wheatley, J. R., Amis, T. C., and Engel, L. A. (1991). Oronasal partitioning of ventilation during exercise in humans. *J. Appl. Physiol.* **71,** 546–551.

Winter, S. M., Weber, G. L., Gooley, P. R., MacKenzie, N. E., and Sipes, I. G. (1992). Identification and comparison of the urinary metabolites of [1,2,3-$^{13}C_3$]acrylic acid and [1,2,3-$^{13}C_3$]propionic acid in the rat by homonuclear ^{13}C nuclear magnetic resonance spectroscopy. *Drug Metab. Dispos.* **20,** 665–672.

Young, J. T. (1981). Histopathologic examination of the rat nasal cavity. *Fundam. Appl. Toxicol.* **1,** 309–312.